

Review

# Design of Functional $Ti_3C_2T_x$ MXene for Gas Sensors and Energy Harvesting: A Review

Qui Thanh Hoai Ta <sup>1,†</sup>, Deepika Thakur <sup>2,†</sup> and Jin-Seo Noh <sup>1,\*</sup>

<sup>1</sup> Department of Physics, Gachon University, 1342 Seongnamdaero, Sujeong-gu, Seongnam-si 13120, Gyeonggi-do, Republic of Korea; tathanhhoaiqui2292@gmail.com

<sup>2</sup> Department of Agriculture, Forestry and Bioresources, Seoul National University, 1 Gwanak-ro, Gwanak-gu, Seoul 08826, Republic of Korea; thakurdeepz80@gmail.com

\* Correspondence: jinseonoh@gachon.ac.kr; Tel.: +82-317505611

† These authors contributed equally to this work.

**Abstract:** Two-dimensional (2D) inorganic compounds, MXenes, are the most promising candidate for chemical sensors and environmental remediation. Since the first synthesis of  $Ti_3C_2T_x$  MXene from the  $Ti_3AlC_2$  MAX phase in 2011, 2D materials have been attracting significant attention from a wide range of scientific communities because of their unique physicochemical properties. The attractive properties of MXenes motivated us to explore the new wave of front-end research and applications. Over the past 12 years, there have been more than 10,000 theoretical and experimental studies on MXenes. All these publications have primarily focused on  $Ti_3C_2T_x$  MXene because of its fascinating material properties and tunability towards target applications. To provide readers with a fundamental understanding of this emerging 2D material, this review discusses the recent trends in the design of  $Ti_3C_2T_x$  MXene for gas sensors and energy harvesting applications. For the most updated information, this review focuses on important findings and applications reported in the last decade.

**Keywords:**  $Ti_3C_2T_x$  MXenes; gas sensors; composites; response; energy harvesting



**Citation:** Ta, Q.T.H.; Thakur, D.; Noh, J.-S. Design of Functional  $Ti_3C_2T_x$  MXene for Gas Sensors and Energy Harvesting: A Review. *Chemosensors* **2023**, *11*, 477. <https://doi.org/10.3390/chemosensors11090477>

Academic Editor: Dan Xie

Received: 26 June 2023

Revised: 29 July 2023

Accepted: 13 August 2023

Published: 1 September 2023



**Copyright:** © 2023 by the authors. Licensee MDPI, Basel, Switzerland. This article is an open access article distributed under the terms and conditions of the Creative Commons Attribution (CC BY) license (<https://creativecommons.org/licenses/by/4.0/>).

## 1. Introduction

Ever-growing power consumption, the accumulative demand for smart materials, and the need for green electronics for low-power and low-voltage devices have led to increased demand to develop alternatives for supercapacitors and batteries, which is exemplified by self-powered wearable microelectronic devices [1–3]. Therefore, it is crucial to find smart materials that can be applied to photocatalysis, electrocatalytic sensors, chemical adsorbents, energy conversion, gas sensors, and biomedical applications. To this end, by the end of 2004, Novoselov et al. [4] actively explored graphene, which is considered the pioneering work of two-dimensional (2D) nanomaterials. Subsequently, an increasing number of 2D nanomaterials such as phosphorene, transition metal dichalcogenides, transition metal carbides/nitrides, and hexagonal boron nitrides have been discovered [5–7]. Among these 2D materials, new 2D materials referred to as MXenes have been at the forefront and become suitable candidates for electrodes, detectors, additives, and separators or hosts for numerous applications because of their outstanding properties [8,9].

Since the first publication on 2D  $Ti_3C_2T_x$  from Drexel University, an increasing number of researchers have focused on producing  $Ti_3C_2T_x$  MXene, demonstrating its attractive qualities, and exploring its diverse applications [10]. The formula for MXenes is  $M_{n+1}X_nT_x$ , where M, X, and  $T_x$  represent an early transition metal (Ta, Hf, Mo, Ti, Mo, Nb, and V), carbon and/or nitrogen, and surface terminations (-OH, -F, =O), respectively;  $n = 1-4$  [11–13]. MXenes have tremendous compositional variety and tunable qualities depending on their structural atomic arrangement, because transition-metal atoms are grouped in a layered pattern with carbon or nitrogen atoms [14–16]. Furthermore, in such atomic sandwiches,

some of the transition-metal atoms are arranged in the surface layers while the remaining metal atoms are placed in the inner layers. Different transition metals can merge into MXenes, such as  $\text{Mo}_2\text{TiC}_2$  or  $\text{Mo}_2\text{Ti}_2\text{C}_3$  [17,18].

As members of the “wonderful material family,” MXenes have been rapidly expanding because of the growing diversity of their parent materials, MAX phases, and advancements in their processing methods [19,20]. The ability to manipulate the structure and morphology of MXenes using multiple methodologies offers the possibility to create a variety of 2D materials with customizable compositions and favorable surface qualities [21–23].

Thus far, more than 35 stoichiometric MXenes have been explored as solid solutions with different combinations of M and X sites recorded [24,25]. From theoretical calculations, a considerably larger number of solid solutions have been obtained, and their experimental syntheses remain pending. A wide range of surface terminations, including Cl, F, O, OH, I, and Br, further expand the number of stoichiometric MXenes, endowing them with unique physical and chemical properties [26–28]. Thus, MXenes have been used in a variety of potential applications, including electromagnetic interference shielding, optoelectronics, photocatalysis, gas sensors, and energy storage [29–31]. Although metallic conductivity facilitates  $\text{Ti}_3\text{C}_2\text{T}_x$  MXene-based chemiresistive gas sensors running at room temperature, gas sensors prepared with pure  $\text{Ti}_3\text{C}_2\text{T}_x$  MXene suffer from poor selectivity (only  $\text{NH}_3$  or VOCs) and low response during gas detection [22,32]. Therefore, integrating  $\text{Ti}_3\text{C}_2\text{T}_x$  MXene with other materials is a promising strategy to enhance catalytic activity, facilitate efficient charge transfer, and reduce energy barriers [33–36]. These effects cooperatively contribute toward enhancing the selectivity of the gas-sensing system and enable operation at room temperature.

Among all MXenes,  $\text{Ti}_3\text{C}_2\text{T}_x$  MXenes offer an exceptionally appealing platform for a wide range of applications, especially for gas sensing and energy harvesting, because of their remarkable electrical qualities and unique tunability. The two applications are important and can stimulate the design of multifunctional  $\text{Ti}_3\text{C}_2\text{T}_x$  MXene-based flexible, high-performance, and cost-effective smart materials. Although there have been several comprehensive reviews on the synthesis, properties, and applications of  $\text{Ti}_3\text{C}_2\text{T}_x$  MXene [37–43], reviews on the detailed and prospective preparation and applications of multifunctional  $\text{Ti}_3\text{C}_2\text{T}_x$  MXene for gas sensors and energy harvesting are very rare. The need for batteries and electrical power sources can be dramatically overcome by combining energy harvesting technologies with gas sensor systems, which also makes the gas sensors more sustainable and easier to deploy in both remote and hard-to-reach locations. In addition, energy harvesting can reduce the maintenance costs of the gas sensors and enhance the overall lifetime of the devices [44–46].

To this end, we highlight recent advances in  $\text{Ti}_3\text{C}_2\text{T}_x$  MXene implementation for gas sensing and energy harvesting in various environments. Using a self-assembly method, rGO-assisted method, and framework-supported method to prepare  $\text{Ti}_3\text{C}_2\text{T}_x$  MXene can efficiently prevent it from stacking together, which promotes the diffusion of toxic gas molecules. Finally, we discuss future research difficulties and techniques to further investigate the unique properties and potential applications of  $\text{Ti}_3\text{C}_2\text{T}_x$  MXenes.

## 2. Synthesis of $\text{Ti}_3\text{C}_2\text{T}_x$ MXene

### 2.1. Etching

The functional group of  $\text{Ti}_3\text{C}_2\text{T}_x$  MXene critically affects its electrical conduction properties, serving as covalent linking sites with other nanostructures and as active sites for adsorbing gas molecules.  $\text{Ti}_3\text{C}_2\text{T}_x$  MXenes are created by selectively etching specific atomic layers from their parent MAX phases, where A is an A group (groups 13 and 14, or IIIA, IVA) of the periodic table [47]. Selective etching is the main experimental method for synthesizing  $\text{Ti}_3\text{C}_2\text{T}_x$  MXene, which has a metallic Ti-Al bond strength weaker than that of Ti-C bonds [48]. Aqueous solutions with the fluoride group have been mostly used to remove Al layers from the  $\text{Ti}_3\text{AlC}_2$  MAX phase, such as direct hydrofluoric acid (HF, 50%) or the in situ creation of HF from lithium fluoride (LiF) and hydrochloric acid (HCl), as

shown in Figure 1 [49–52]. Both ammonium fluoride ( $\text{NH}_4\text{F}$ ) and ammonium hydrogen bifluoride ( $\text{NH}_4\text{HF}_2$ ) have also been effectively applied for making  $\text{Ti}_3\text{C}_2\text{T}_x$  MXene. Only Al has been effectively removed from MAX phases from the 12 elements of groups 13 and 14. The chemical reactions that happen during the HF etching of the  $\text{Ti}_3\text{AlC}_2$  MAX phase are given below [53–55]:

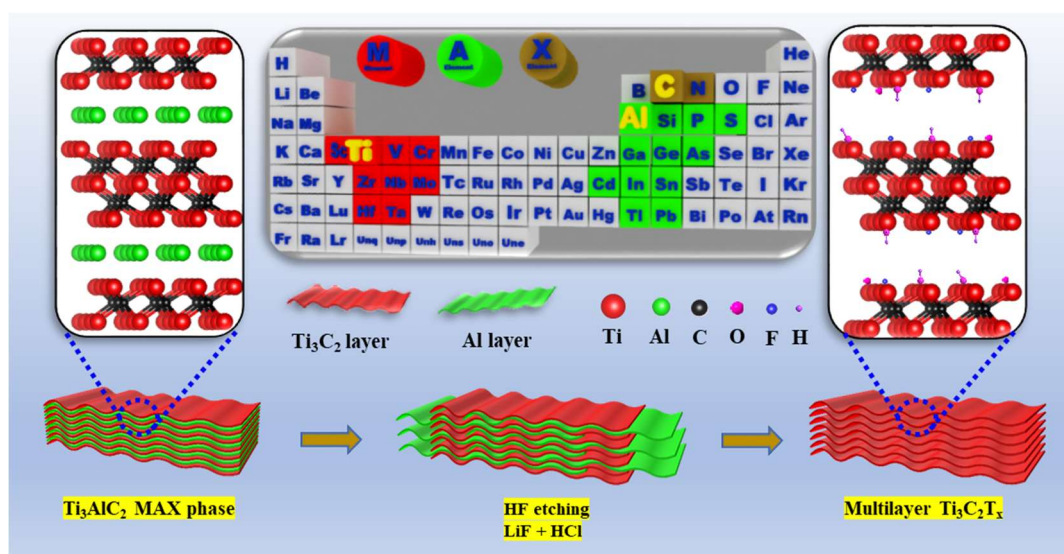
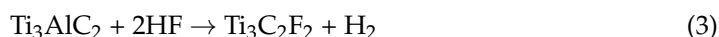
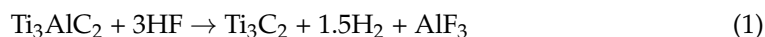


**Figure 1.** Schematic of  $\text{Ti}_3\text{C}_2\text{T}_x$  MXene preparation from the  $\text{Ti}_3\text{AlC}_2$  MAX phase. Reprinted and adapted with permission from [11]. Copyright 2021, Elsevier.

There is another technique to prepare MXenes from nonMAX phases, which is etching aluminum carbide ( $\text{Al}_3\text{C}_3$ ) from a nonMAX phase. In this nonMAX phase precursor, Al-C units separate either  $\text{M}_3\text{C}_2$  or  $\text{M}_2\text{C}$  layers, e.g.,  $\text{U}_2\text{Al}_3\text{C}_3$ .  $\text{Mo}_2\text{CT}_x$  MXenes have also been prepared via Ga layer etching from  $\text{Mo}_2\text{Ga}_2\text{C}$  [10,56–58]. MXenes can be synthesized using molten fluoride salt at high temperatures, as demonstrated by the synthesis of  $\text{Ti}_4\text{N}_3$  from  $\text{Ti}_4\text{AlN}_3$  at  $550^\circ\text{C}$  under Ar flow. The  $\text{TiC}_x$  nanostructure was synthesized by annealing a mixture of molten LiF and  $\text{Ti}_2\text{AlC}$  at  $900^\circ\text{C}$  [59]. This method was not efficient and removed either the M or A element because of the specific treatment environment. These results and the morphologies of  $\text{Ti}_3\text{C}_2\text{T}_x$  MXene suggest that the aqueous fluoride-containing acidic technique is suitable for synthesizing  $\text{Ti}_3\text{C}_2\text{T}_x$  MXenes. Moreover, etching in the presence of a metal halide such as LiF tends to intercalate the cation ( $\text{Li}^+$ ) and water, increasing the distance between each layer [60–63].

Halogen etching is a new technique for preparing  $\text{Ti}_3\text{C}_2\text{T}_x$  MXene. In 2021, Jawaid et al. [64] explored an etching method to prepare  $\text{Ti}_3\text{C}_2\text{T}_x$  MXene using halogens ( $\text{IBr}$ ,  $\text{ICl}$ ,  $\text{I}_2$ ,  $\text{Br}_2$ ) in anhydrous media. The halogen-based etching is conducted in a glove box for 8 h with an inert ambient ( $\text{H}_2\text{O}:\text{O}_2$  was around 1:3) at room temperature, as shown in Figure 2. The recommended mechanism implies that continual halogen addition will provide reaction productivity and increase the yield of halogenated  $\text{Ti}_3\text{C}_2\text{X}_n$  with halogen-terminated surfaces ( $\sim 1\%$  yield of MXene on 1 mg/mL). The etching process with different halogens led to a variety of halogen-terminated surfaces ( $\text{X} = \text{Br}, \text{I}, \text{C}, \text{F}$ ) at room temperature. A low-dielectric organic solution was used to obtain the purified size-selected  $\text{Ti}_3\text{C}_2\text{X}_n$  MXene. In the same context, a fluoride-free  $\text{Ti}_3\text{C}_2\text{T}_x$  MXene with O-rich terminal groups was generated using an iodine-assisted etching method in anhydrous acetonitrile

(CNCH<sub>3</sub>) [65]. The Al layer was removed from the MAX phase by iodine because the Ti-C bond is stronger than Ti-Al. The I<sub>2</sub>-etched MXene was washed several times using a 1 M HCl solution to dissolve AlI<sub>3</sub> and exfoliate multilayer Ti<sub>3</sub>C<sub>2</sub>T<sub>x</sub> MXene by manual shaking. The I<sub>2</sub>-etched Ti<sub>3</sub>C<sub>2</sub>T<sub>x</sub> MXene has excellent conductivity (1250 S/cm), ultimate thickness (5 nm), and large size (1.8 μm) with oxygen-rich termination groups. These abundant oxygen functional groups are good for gas-sensing performance and energy storage because they act as active sites and take up hydrogen ions.

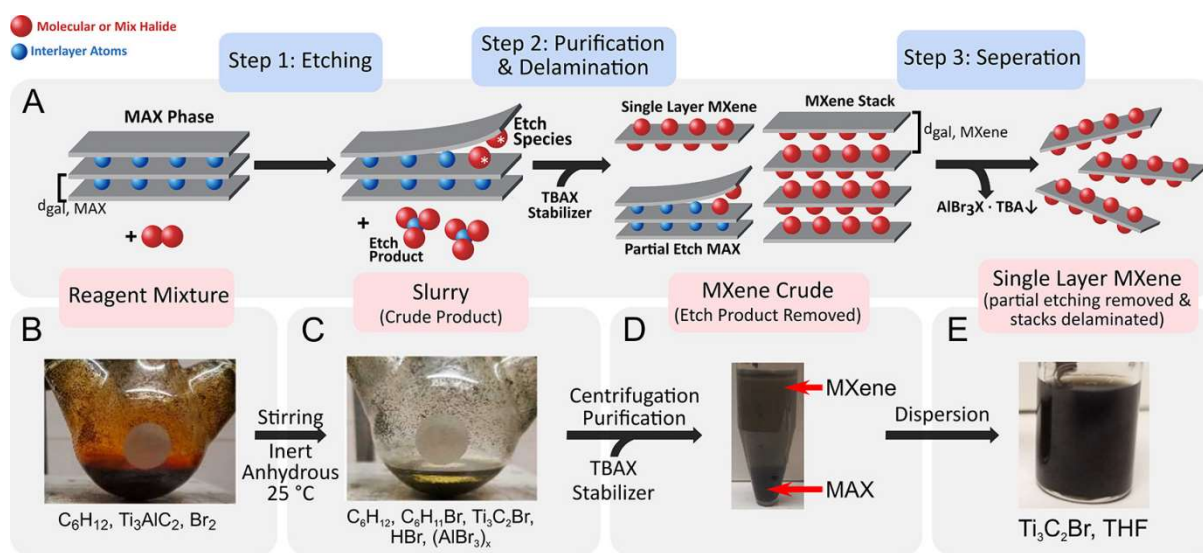


**Figure 2.** (A–E) Halogen etching procedure of the MAX phase. Tetrahydrofuran was used as the stable colloidal solution. Reprinted and adapted with permission from [64]. Copyright 2021 American Chemical Society.

Yang et al. [66] prepared Ti<sub>3</sub>C<sub>2</sub>T<sub>x</sub> using NH<sub>4</sub>Cl and tetramethylammonium hydroxide (TMA.OH) using electrochemical etching with low potential (+5 V). The exfoliated single-layer and bilayer Ti<sub>3</sub>C<sub>2</sub>T<sub>x</sub> MXenes were collected with high yield (90%) because of the delamination of the positive charge ions (TMA<sup>+</sup>) and as Cl<sup>−</sup> ions have a strong binding with Al. This technique does not require any dangerous F-containing agents, and the Al layers are replaced by hydroxide and the oxygen group. The average lateral size of the obtained Ti<sub>3</sub>C<sub>2</sub>T<sub>x</sub> MXene is ~2 μm, which is larger than that of the traditional HF etching process. This method offers a safe technique to scale the preparation of Ti<sub>3</sub>C<sub>2</sub>T<sub>x</sub> MXene. In 2018, Tengfei et al. [67] attempted to directly utilize 27.5 M NaOH to etch 100 mg of the Ti<sub>3</sub>AlC<sub>2</sub> MAX phase in an Ar atmosphere with excellent efficiency (92 wt%). The obtained samples were synthesized at 270 °C via alkali treatment and had a (002) plane spacing of 23.4 Å, which was larger than that of Ti<sub>3</sub>C<sub>2</sub>T<sub>x</sub> prepared using an HF-related technique. This technique offers an alkali etching process for Ti<sub>3</sub>C<sub>2</sub>T<sub>x</sub> MXene in which the pure MAX phase must be uninvolved. Moreover, Ti<sub>3</sub>C<sub>2</sub>T<sub>x</sub> MXene can be cationized with poly(diallyldimethylammonium chloride) (PDDA) as a stabilizer to better compound with negatively charged materials through self-reduction and/or electrostatic interaction [68].

## 2.2. Delamination

Delaminating any 2D material is important for achieving interlayer interaction. Ti<sub>3</sub>C<sub>2</sub>T<sub>x</sub> MXenes can be intercalated and exfoliated in polar organic molecules, followed by manual shaking or mechanical vibration in water to obtain monolayer and few-layer Ti<sub>3</sub>C<sub>2</sub>T<sub>x</sub> MXenes. Ultrasonication is the main tool for separating and delaminating Ti<sub>3</sub>C<sub>2</sub>T<sub>x</sub> MXene sheets with precision to dramatically accelerate the procedure and process an advanced fraction of high-quality nanosheets. Ti<sub>3</sub>C<sub>2</sub>T<sub>x</sub> can be exfoliated with dimethyl sulfoxide (DMSO) or tetrabutylammonium hydroxide (TBAOH) by manual shaking, and it can

then be filtered to obtain the freestanding MXene “paper” [16,27,69]. Etching the  $\text{Ti}_3\text{AlC}_2$  MAX phase in the presence of a fluoride salt makes it easy to obtain few-layer  $\text{Ti}_3\text{C}_2\text{T}_x$  MXene without any delamination step because of the effect of metal cations in halide salts (Figure 3) [70–72].

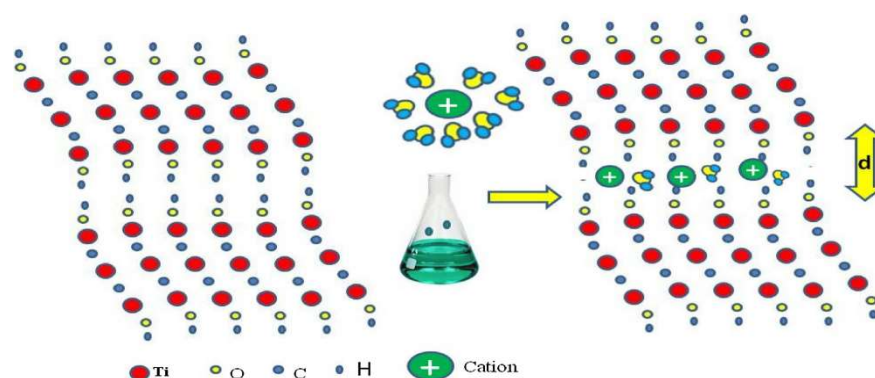


**Figure 3.** Schematic of an increase in the  $d$ -spacing of  $\text{Ti}_3\text{C}_2\text{T}_x$  MXene with intercalation using cations. Reprinted and adapted with permission from [70].

The resistance of  $\text{Ti}_3\text{C}_2\text{T}_x$  MXene without intercalation is smaller than that with intercalation because intercalation-induced interlayer swelling retards the out-of-plane electron transport. Metal ion intercalation is one of the effective techniques for improving the diffusion coefficients of gas molecules and ionic species [16,73]. Consequently, scientists focused on using metal ion intercalation to enhance the gas-sensing performance and the energy storage activity of  $\text{Ti}_3\text{C}_2\text{T}_x$  MXene-based composites. The enhanced gas-sensing mechanism of metallic  $\text{Ti}_3\text{C}_2\text{T}_x$  MXene is more sophisticated than the electron movement and surface adsorption in traditional 2D materials. Suitable cation exfoliation can contribute to the swelling of  $\text{Ti}_3\text{C}_2\text{T}_x$  MXene, which can improve the conductivity change when exposed to reducing gases or oxidizing gases.

### 3. Structure and Properties

$\text{Ti}_3\text{AlC}_2$  is the most commercially available, low-cost MAX phase for producing  $\text{Ti}_3\text{C}_2\text{T}_x$  MXene with superior metallic conductivity and low diffusion barriers. In terms of electrical properties,  $\text{Ti}_3\text{C}_2\text{T}_x$  MXenes were almost like multilayer graphene. The conventional HF-etched  $\text{Ti}_3\text{C}_2\text{T}_x$  MXene and additive-free  $\text{Ti}_3\text{C}_2\text{T}_x$  MXene film have shown volumetric capacitances around 300 F and 1500 F per cubic centimeter, respectively [74,75]. In addition, the multilayered structure of  $\text{Ti}_3\text{C}_2\text{T}_x$  MXene provides a high cycling rate and stability. Benefitting from the electronic sensitization and synergistic effect of Ti on MXenes, the charge carrier transportation, response, and other electrical parameters of  $\text{Ti}_3\text{C}_2\text{T}_x$  MXene-based electrical devices can be enhanced significantly.

Similar to its parent,  $\text{Ti}_3\text{C}_2\text{T}_x$  MXene has a hexagonal close-packed structure, and the C atoms occupy the octahedral interstitial sites composed of 6 Ti atoms.  $\text{Ti}_3\text{C}_2\text{T}_x$  MXenes are prepared using hydrofluoric acid and have surface functional groups  $\text{T}_x$  (-OH, -F, =O). Moreover, they can have another kind of  $\text{T}_x$ , such as -Cl, -Br, and -I, when different etching and delaminating agents are employed [76–78].

The etchant plays a crucial role in the delamination quality of MXene. For example, a HF-etched  $\text{Ti}_3\text{C}_2\text{T}_x$  has thicker multilayer lamellas and narrower interstack gaps than those of (LiF + HCl)-etched  $\text{Ti}_3\text{C}_2\text{T}_x$ . The space between each layer of (LiF + HCl)-etched  $\text{Ti}_3\text{C}_2\text{T}_x$  is around 2.8 Å due to the presence of metal cation, which is larger than that of HF-etched  $\text{Ti}_3\text{C}_2\text{T}_x$  MXene [79]. The product from a lower HF concentration yields a larger O:F ratio [80–83]. For the removal of the Al layer in the  $\text{Ti}_3\text{AlC}_2$  MAX phase, at least 18 h of HF etching (30 wt%) is necessary, which was established by the shift of a main peak ((002) peak) from 9.5° to 9.0° in the XRD measurement, as shown in Figure 4. In fact,  $\text{Ti}_3\text{C}_2\text{T}_x$

MXenes with less open structures were collected when etched with HF solutions of 5 wt% and 10 wt% for 24 h and 18 h [5].

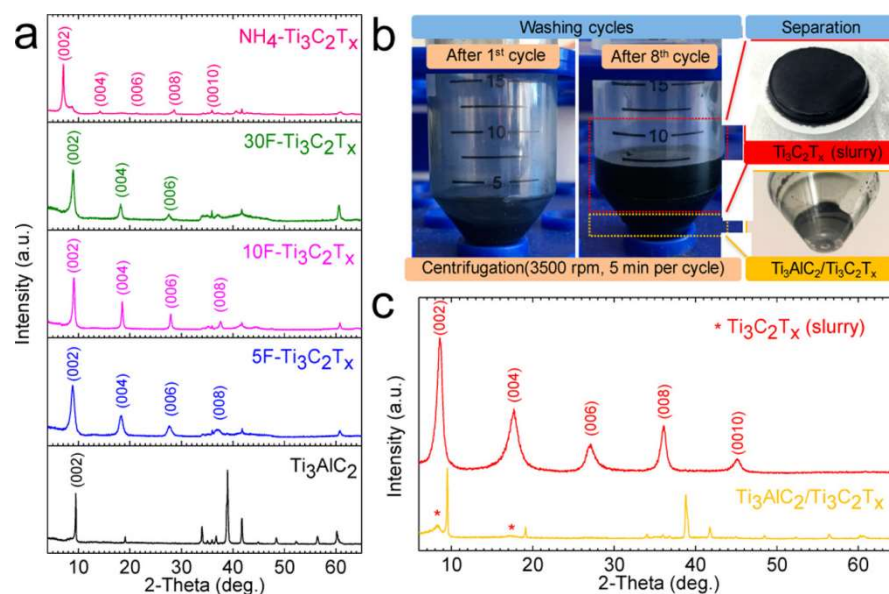


**Figure 4.** (a–c) XRD results of Ti<sub>3</sub>C<sub>2</sub>T<sub>x</sub> MXene prepared with different concentrations of HF solution. Reprinted and adapted with permission from [5]. Copyright 2017 American Chemical Society.

Multilayer Ti<sub>3</sub>C<sub>2</sub>T<sub>x</sub> MXenes are not stable in an ambient environment with water and oxygen molecules; however, they are stable in dry air and oxygen-free degassed water. Consequently, it is highly recommended to store Ti<sub>3</sub>C<sub>2</sub>T<sub>x</sub> MXene colloids at low temperatures in refrigerators and in dark environments. Further, the standard manufacturing procedure yields high-quality Ti<sub>3</sub>C<sub>2</sub>T<sub>x</sub> MXene with high stability [84–87]. However, Ti<sub>3</sub>C<sub>2</sub>T<sub>x</sub> MXene powders can be stored in a vacuum environment; vacuum drying or lyophilization can be active in preserving MXene powders, because they eliminate the solvent and reduce the potential for deprivation or agglomeration. In terms of suitability during experiments, using Ti<sub>3</sub>C<sub>2</sub>T<sub>x</sub> MXene powder can have certain advantages over colloidal suspensions.

#### 4. Applications of Ti<sub>3</sub>C<sub>2</sub>T<sub>x</sub> MXenes in Gas Sensors

The main function of gas sensors is to detect gases at low concentrations (ppm, ppb, or even ppt level), which are lower than the recognition of the nose olfactory nerve. In industry, gas-sensing devices are utilized to control the concentration of toxic gases such as volatile organic compounds (VOCs), NO<sub>2</sub>, and H<sub>2</sub>S to guarantee that the working atmosphere is safe for workers. Moreover, it can also be used to control the concentration of explosive and flammable gases. The gas-sensing material plays the main role in the operation of gas sensors, which should be normally stable; however, they should sensitively respond to target gases at room temperature. The gas sensor response is determined by calculating the relative change in the sensor material's resistance in an air environment ( $R_{air}$ ) versus its resistance in the specific gas being tested ( $R_{gas}$ ) after the injection of gas. The calculation is

$$\text{Response}(\%) = \frac{R_{gas} - R_{air}}{R_{air}} \times 100 \quad (4)$$

##### 4.1. MXene Gas Sensors

Multilayered Ti<sub>3</sub>C<sub>2</sub>T<sub>x</sub> MXene has been considered a potential candidate for gas sensors because of its large surface area, high electrical conductivity, and wealthy surface functional groups that can act as active sites. Ti<sub>3</sub>C<sub>2</sub>T<sub>x</sub> MXene provides an excellent path for electron transport at room temperature because of its metallic conductivity, which results in enhanced gas-sensing signals [87–92]. Table 1 shows that pure Ti<sub>3</sub>C<sub>2</sub>T<sub>x</sub> MXene and

$\text{Ti}_3\text{C}_2\text{T}_x$  composites can interact with various toxic gas molecules with a good response and fast recovery time. The resistance of metallic  $\text{Ti}_3\text{C}_2\text{T}_x$  MXene was almost increased when exposed to a toxic gas in both oxidizing and reduced gas environments at room temperature [6,38,93,94]. One study by Lipatov et al. [94] examined the effect of different gas environments on the electrical conductivity of  $\text{Ti}_3\text{C}_2\text{T}_x$  MXene films. The authors discovered that exposure to ambient air, which can be classified as an oxidizing environment, led to an increase in the resistance of the MXene films because of the formation of a thin surface oxide layer. Unlike the rise in resistance in oxidizing environments, several studies have shown that  $\text{Ti}_3\text{C}_2\text{T}_x$  MXenes exhibit enhanced electrical conductivity in reducing gas environments [95–97]. For example, Doan et al. [95] revealed that the electrical conductivity of  $\text{Ti}_3\text{C}_2\text{T}_x$  MXene films massively increased upon exposure to hydrogen gas, which acts as a reducing agent. A convincing gas-sensing mechanism of metallic  $\text{Ti}_3\text{C}_2\text{T}_x$  MXene needs to be developed to fully understand the sensing process and create a breakthrough for further applications of  $\text{Ti}_3\text{C}_2\text{T}_x$  MXenes.

**Table 1.** Gas-sensing activities of pure  $\text{Ti}_3\text{C}_2\text{T}_x$  MXenes and their composites.

Materials	Gas	Temperature (°C)	Concentration (ppm)	Response (%)	$t_{\text{Res}}/t_{\text{Rec}}$ (s)	Reference
$\text{Ti}_3\text{C}_2\text{T}_x$	Acetone	RT	5	3.7	91/103	[98]
$\text{Ti}_3\text{C}_2\text{T}_x$	$\text{NH}_3$	RT	100	28.88	1/201	[99]
$\text{Ti}_3\text{C}_2\text{T}_x/\text{CuO}$	Toluene	250	50	11.5	270/10	[100]
$\text{Ti}_3\text{C}_2\text{T}_x@\text{TiO}_2@\text{MoS}_2$	$\text{NO}_2$	RT	50	55.1	1.8/70	[101]
$\text{Ti}_3\text{C}_2\text{T}_x/\text{SnO}_2$	$\text{NH}_3$	RT	50	41	36/45	[102]
$\text{Ti}_3\text{C}_2\text{T}_x/\text{MoS}_2$	$\text{NO}_2$	RT	10	25.1	530/140	[103]
$\text{Ti}_3\text{C}_2\text{T}_x/\text{MoS}_2$	$\text{NO}_2$	RT	20	40.1	525/155	[103]
$\text{Ti}_3\text{C}_2\text{T}_x/\text{Co}_3\text{O}_4$	HCHO	RT	10	9.3	84/6	[104]
$\text{Ti}_3\text{C}_2\text{T}_x/\text{ZnO}$	$\text{NO}_2$	RT	20	22.3	34/103	[105]
$\text{Ti}_3\text{C}_2\text{T}_x/\text{WO}_3$	$\text{NH}_3$	RT	1	22.4	120/229	[106]
$\text{Ti}_3\text{C}_2\text{T}_x/\text{PANI}$	Ethanol	RT	200	42	0.4/0.5	[107]
$\text{Ti}_3\text{C}_2\text{T}_x/\text{W}_{18}\text{O}_{49}$	Acetone	300	0.18	1.4	5.7/7	[108]
$\text{Ti}_3\text{C}_2\text{T}_x/\text{PEDOT:PSS}$	$\text{NH}_3$	RT	100	37	117/40	[109]
$\text{Ti}_3\text{C}_2\text{T}_x/\text{In}_2\text{O}_3$	Methane	RT	5	30	6.6/4	[110]
$\text{Ti}_3\text{C}_2\text{T}_x/\text{SnS}_2$	$\text{NO}_2$	RT	1000	116	65/10	[111]
$\text{Ti}_3\text{C}_2\text{T}_x/\text{WSe}_2$	Ethanol	RT	40	25	10/6	[112]
$\text{Ti}_3\text{C}_2\text{T}_x/\text{GO}$	$\text{NH}_3$	RT	100	8	-/-	[113]
$\text{Ti}_3\text{C}_2\text{T}_x/\text{Co}_3\text{O}_4/\text{PEI}$	$\text{NO}_x$	RT	100	30	2/74	[114]
$\text{Ti}_3\text{C}_2\text{T}_x/\text{Fe}_2(\text{MnO}_4)_3$	N-butane	RT	100	44	19/25	[115]

Among the members of the MXene family of 2D materials, a considerable amount of research has been performed on  $\text{Ti}_3\text{C}_2\text{T}_x$  MXene to establish its synthesis routine and unveil its qualities [116,117]. Lee et al. [118] developed a gas sensor using  $\text{Ti}_3\text{C}_2\text{T}_x$  MXene; the sensor displayed good sensing performance to ammonia, ethanol, methanol, and acetone at room temperature. For their study,  $\text{Ti}_3\text{C}_2\text{T}_x$  MXene was prepared using 9 M HCl and 1 g of LiF at 35 °C, and a flexible polyimide film was used as the gas-sensing substrate (Figure 5). The average response signals of the as-prepared material were 7.5, 11.5, 14.3, and 21% for 100 ppm of acetone, ethanol, methanol, and ammonia, respectively. All response signals of  $\text{Ti}_3\text{C}_2\text{T}_x$  had positive signs for all types of gases, suggesting that MXene behaved like a p-type material. Thus, the p-type behavior resulted from oxygen and water molecules introduced during the etching process, which may have acted as the main active sites and received electrons from the electron-donating gases, leading to a drop in the majority carrier population. Thanh et al. [95] constructed palladium-decorated  $\text{Ti}_3\text{C}_2\text{T}_x$  MXene using a polyol method to combine 1D Pd nanoparticles with multilayered  $\text{Ti}_3\text{C}_2\text{T}_x$  MXene for multifunctional operation as hydrogen storage and a  $\text{H}_2$  gas sensor. The responses of the Pd- $\text{Ti}_3\text{C}_2\text{T}_x$  composite to 10, 50, and 100 ppm of  $\text{H}_2$  were recorded at 10, 20, and 25%, respectively. The enhanced responses of optimized Pd- $\text{Ti}_3\text{C}_2\text{T}_x$  composite could be ascribed

to the roles of Pd NPS and the aforementioned O functional groups of MXene, which may collaboratively supply H atoms to a nearby composite via a spill-over mechanism.

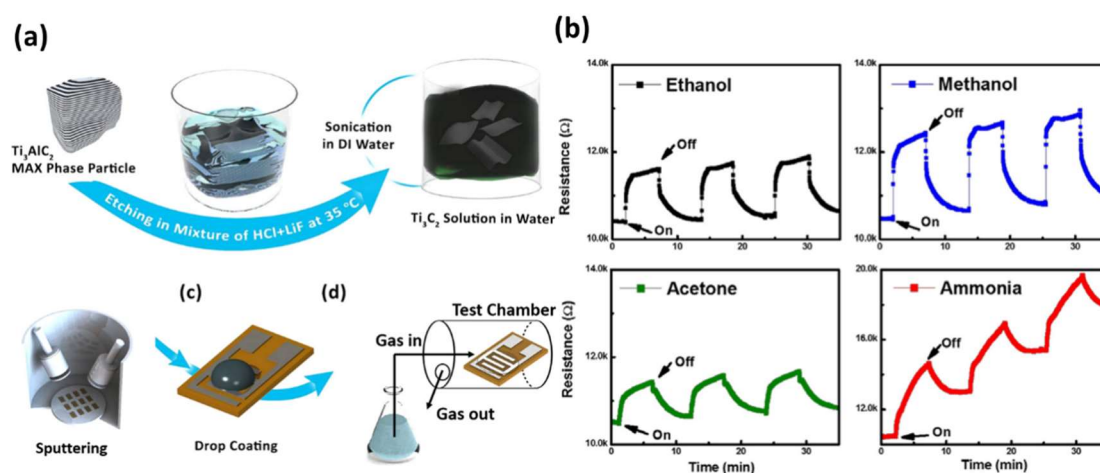


**Figure 5.** (a,c,d) Schematic of the  $Ti_3C_2T_x$  gas-sensing material and (b) its sensing signals of various toxic gases of 100 ppm at room temperature. Reprinted and adapted with permission from [118]. Copyright 2017 American Chemical Society.

Kim et al. [32] reported that the  $Ti_3C_2T_x$  MXene gas sensor exhibits high sensitivity to volatile organic compounds with a very low detection limit (50 ppb) at room temperature. The sensor's signal-to-noise ratio was extremely high, twice as large as that for other sensing materials. The response values of  $Ti_3C_2T_x$  films on exposure to 100 ppm of  $SO_2$ ,  $NO_2$ , propanol, ammonia, ethanol, and acetone were 0.16, 0.21, 0.88, 0.80, 1.76, and 1.18%, respectively. The low noise of the as-prepared  $Ti_3C_2T_x$  MXene can be attributed to the high electrical conductivity and structural uniformity obtained by the vacuum-filtrated technique, which has a comparative advantage over other techniques such as drop-casting.  $Ti_3C_2T_x$  MXene with a small thickness (25 nm) showed good sensitivity compared to MXenes with 50 and 150 nm thicknesses; this is strongly correlated with the fraction of active sites exposed on the surface (Figure 6). They demonstrated that the highly conductive  $Ti_3C_2T_x$  MXene could be used to sense different VOCs with clear response signals and low electrical noise, realized by the support of the hydroxyl and oxygen groups. According to the DFT calculations,  $Ti_3C_2(OH)_2$  showed the toughest binding energy strengths (1.2 Å and  $-0.774$  eV for acetone), stronger than those of other functional groups.

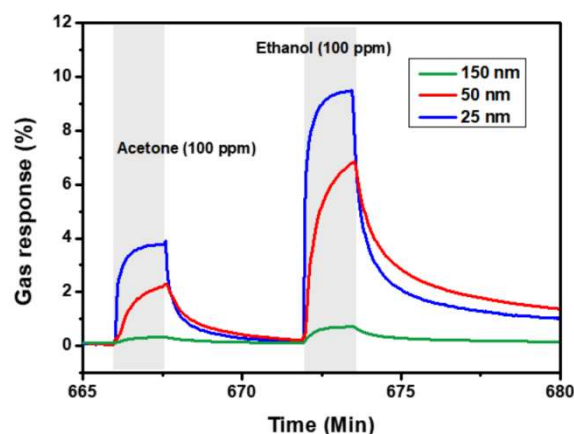


**Figure 6.** Thickness-dependent responses of  $Ti_3C_2T_x$  MXene to various gases at a fixed concentration of 100 ppm. Reprinted and adapted with permission from [32].

Sanjit et al. [119] prepared accordion-like- $\text{Ti}_3\text{C}_2\text{T}_x$  MXene from  $\text{Ti}_3\text{AlC}_2$  via 48% HF etching for 15 h at 60 °C. The as-prepared  $\text{Ti}_3\text{C}_2\text{T}_x$  MXene displayed a macroscopic layer separation of 200 nm. The resistance changed positively when the  $\text{Ti}_3\text{C}_2\text{T}_x$  sensor was exposed to acetone at room temperature. The responses to 100 ppm and 0.25 ppm of acetone vapor were 99%, and 17.3% with a fast response time (53 s), respectively. The hydrogen bonding on the surface of MXene facilitated acetone-molecule interactions with the sensor material. The O and C atoms in acetone gas strongly bound to the  $\text{Ti}_3\text{C}_2\text{T}_x$  MXene surface. Multilayered  $\text{Ti}_3\text{C}_2\text{T}_x$  MXene seems to promote a higher surface area and possibly a higher gas adsorption capacity. Low-layered  $\text{Ti}_3\text{C}_2\text{T}_x$  MXene offers faster response times, higher sensitivity, and better accessibility to gas molecules, but with a lower surface area and potential stability. The choice between these  $\text{Ti}_3\text{C}_2\text{T}_x$  MXene alternatives depends on the specific requirements of gas-sensing applications.

Winston et al. [120] studied functionalizing multilayered  $\text{Ti}_3\text{C}_2\text{T}_x$  with a superhydrophobic protection layer using fluoroalkylsilane functionalization. The optimized sample provided a superhydrophobic surface and enabled the sensor to operate normally even in humid environments. The sensor yielded responses of 3, 5, and 14% to 5, 15, and 120 ppm of ethanol, respectively. The improved responses could be attributed to local structure deformation and adjacent oxygen atoms.

In 2020, Shoumya et al. [121] doped  $\text{Ti}_3\text{C}_2\text{T}_x$  MXene with sulfur to design a room temperature VOCs sensor. In their report,  $\text{Ti}_3\text{C}_2\text{T}_x$  MXene was mixed with thiourea as a sulfur source, and then heated to 500 °C under Ar flow. The optimal S-doped  $\text{Ti}_3\text{C}_2\text{T}_x$  MXene showed an excellent response (12%) to 1 ppm toluene with long-term stability (1 month). The -S functional groups play a key role for enhanced gas sensing, which is modified upon doping, thereby increasing the binding energy of gas molecules substantially.

Wu et al. [22] used dimethyl sulfoxide to synthesize single-layered  $\text{Ti}_3\text{C}_2\text{T}_x$  MXene for toxic gas detection at room temperature. Among the eight different gases, the response signal for  $\text{NH}_3$  was 6.1%, which is four times the response for ethanol (1.5%). The selectivity of the  $\text{NH}_3$  chemiresistive gas sensor was higher than others because of the clean surface of the microstructure of  $\text{Ti}_3\text{C}_2\text{T}_x$  MXene, which had a higher adsorption area when using HCl and NaF as the etchant. The potential of  $\text{Ti}_3\text{C}_2\text{T}_x$  MXene for  $\text{NH}_3$  detection was demonstrated using first-principles calculation. The authors indicated that O-terminated  $\text{Ti}_3\text{C}_2\text{T}_x$  was the most energetically favorable compared to the F-terminated  $\text{Ti}_3\text{C}_2\text{T}_x$  and OH-terminated  $\text{Ti}_3\text{C}_2\text{T}_x$ . The calculations displayed that the adsorption energy of  $\text{NH}_3$  (−0.078 eV/atom) has a considerably stronger interaction with O-terminated  $\text{Ti}_3\text{C}_2\text{T}_x$  than that of  $\text{CH}_4$  (−0.022 eV/atom),  $\text{H}_2\text{S}$  (−0.047 eV/atom). Further, the N atom in the  $\text{NH}_3$  molecules lies straight above the Ti atom in O-terminated  $\text{Ti}_3\text{C}_2\text{T}_x$  (Figure 7). The adsorbed geometry and adsorption energy results guarantee that the response of  $\text{NH}_3$  molecules is considerably better than those of other toxic gases; the O-terminated  $\text{Ti}_3\text{C}_2\text{T}_x$  MXene has a high selectivity to ammonia at room temperature.

Machine learning was applied to predict the appearance of VOCs molecules on the  $\text{Ti}_3\text{C}_2\text{T}_x$  MXene-based multivariable sensor [122]. Eight different gases with concentrations from 100 to 800 ppm were used as the original data set (Toluene (TOL), methanol (MeOH), hexane, ethanol (EtOH), dichloromethane (DCM), acetone, acetonitrile (MeCN), and isopropanol (IPA)). The principal component analysis (PCA) and linear discrimination analysis (LDA) were executed as supervised pattern recognition tools. Therefore, the VOC mixtures were well separated and had high data dimensionality. The correct cross-validation value of 90.9% was reached, and it revealed that utilizing the  $\text{Ti}_3\text{C}_2\text{T}_x$  MXene-based multivariable gas sensor is a potential method for detecting pure VOCs.

Very few studies have focused on the gas-sensing performance of other kinds of MXenes than  $\text{Ti}_3\text{C}_2\text{T}_x$  MXene. For example, Lee et al. [123] demonstrated the great performance of metallic  $\text{V}_2\text{CT}_x$  MXene gas sensors towards methane and hydrogen with ultrahigh sensitivity at room temperature. Methane has high enthalpy (C-H bonds) and nonpolarity, therefore, it is tremendously difficult to sense the gas at room temperature. Multilayered  $\text{V}_2\text{CT}_x$  MXenes were prepared by Al etching from the  $\text{V}_2\text{AlC}$  MAX phase with

HF acid. Monolayer  $V_2CT_x$  MXene flakes were collected via tetra n-butyl ammonium cation delamination. The gas responses of monolayer  $V_2CT_x$  MXene flakes are estimated to be 1.67% and 0.5% for methane and hydrogen sulfide, respectively (Figure 8). The outstanding detection of  $V_2CT_x$  MXene is related to the oxygen-containing termination groups.

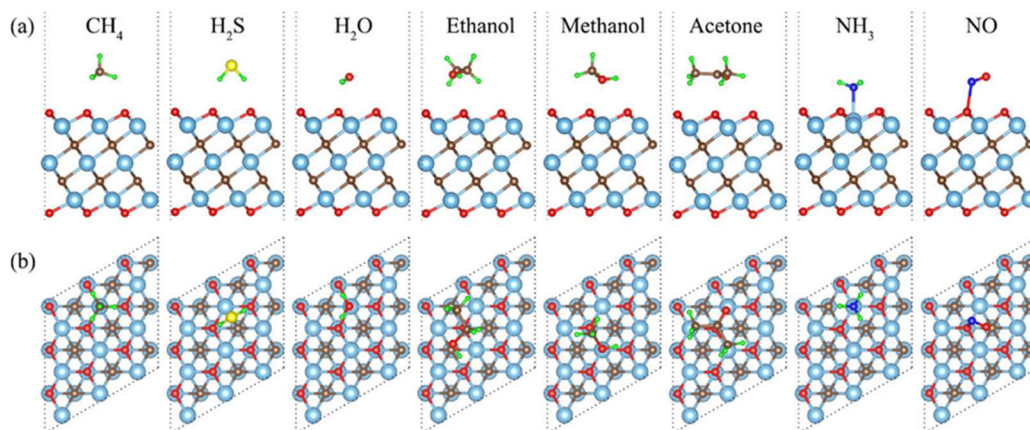


**Figure 7.** (a,b) Side and top views of the optimized structure of eight gas molecules adsorbed on  $Ti_3C_2T_x$  MXene. Reprinted and adapted with permission from [22]. Copyright 2019 American Chemical Society.

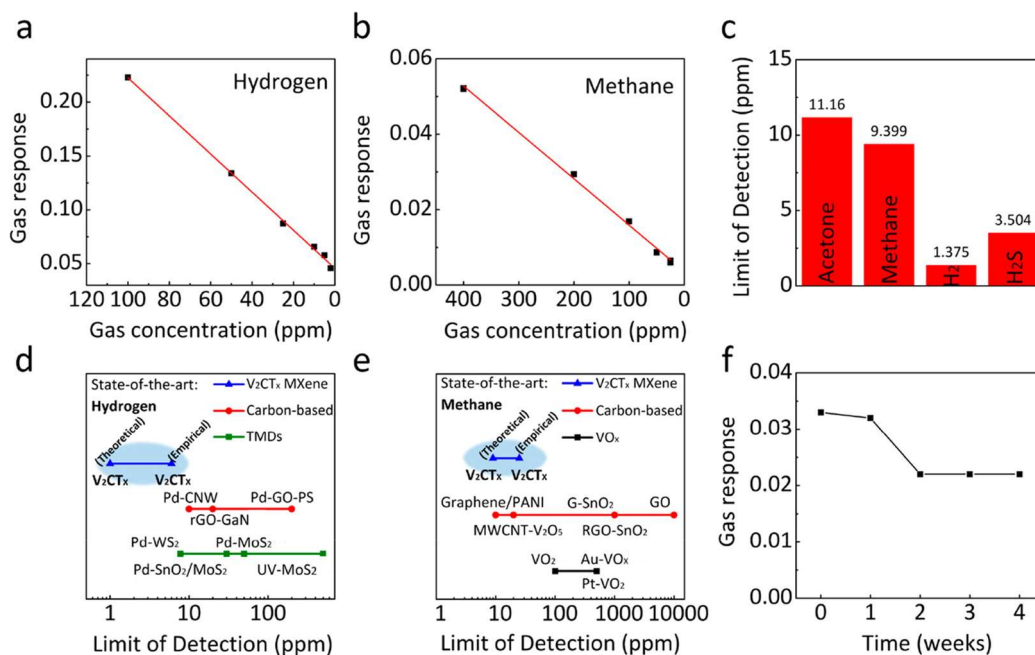


**Figure 8.** (a–f) Gas response variation of monolayer  $V_2CT_x$  MXene flakes to different types of gases. Reprinted and adapted with permission from [123]. Copyright 2019 American Chemical Society.

A toluene sensor using 2D MXene  $Mo_2CT_x$  was studied by Wenzhe et al. [124]. The as-obtained sample successfully detected VOCs with an LOD of 220 ppb at room temperature. The response to acetone, methanol, toluene, ethanol, and benzene was 0.14, 0.58, 2.81, 0.73, and 0.97%, respectively, indicating that  $Mo_2CT_x$  MXene was selective toward toluene compared to other VOCs. The detecting mechanism of the sensor material was based on the interaction between  $Mo_2CT_x$  flakes and the benzene ring in VOCs molecules, which reduces the number of charge carriers. The methyl group further enhance the activity of the phenyl ring in toluene molecules, supporting the evidence that toluene displays the highest response compared to other gases.

#### 4.2. MXene Composites with Chalcogenides and Conductive Polymers

Le et al. [125] researched the effect of transition metal dichalcogenides on  $\text{Ti}_3\text{C}_2\text{T}_x$  MXene for gas-sensing activity.  $\text{WO}_3/\text{Ti}_3\text{C}_2\text{T}_x$  and  $\text{MoS}_2/\text{Ti}_3\text{C}_2\text{T}_x$  composites were prepared by conducting a hydrothermal reaction for 8 h at 170 °C. As shown in Figure 9, the  $\text{MoS}_2$ -covered  $\text{Ti}_3\text{C}_2\text{T}_x$  MXene exhibited great sensitivity to 10 ppm of  $\text{NO}_2$  gas (response = 35%), which was two-fold higher than that of the  $\text{WO}_3/\text{Ti}_3\text{C}_2\text{T}_x$  composite (16%) at the same conditions. The enhanced  $\text{NO}_2$ -sensing capability of  $\text{MoS}_2/\text{Ti}_3\text{C}_2\text{T}_x$  composites can be explained based on the excellent interaction between  $\text{MoS}_2$  and  $\text{Ti}_3\text{C}_2\text{T}_x$  MXene. Many S-terminated edges with high  $d$  electron density can facilitate active electronic interactions with  $\text{NO}_2$  molecules. The electron donation movement can be addressed as

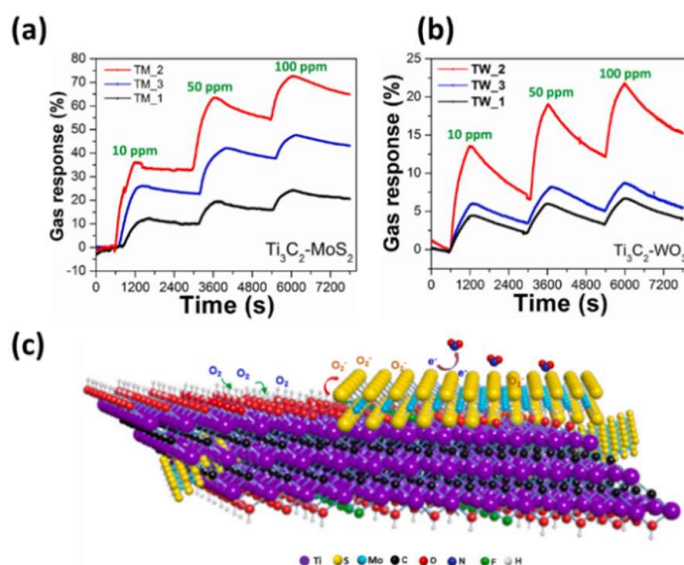


**Figure 9.** (a,b) Comparison of the response behaviors of  $\text{MoS}_2/\text{Ti}_3\text{C}_2\text{T}_x$  and  $\text{WO}_3/\text{Ti}_3\text{C}_2\text{T}_x$  composites to  $\text{NO}_2$  gas. (c)  $\text{NO}_2$ -sensing mechanism of  $\text{MoS}_2/\text{Ti}_3\text{C}_2\text{T}_x$  composite. Reprinted and adapted with permission from [125].

The conductive polymer is suitable for improved gas sensing because of its high sensitivity, high flexibility, and facile fabrication. Therefore, combining  $\text{Ti}_3\text{C}_2\text{T}_x$  MXenes with conductive polymers to create nanocomposites is a good strategy in the field of wearable devices [107,126]. Further, heterojunctions and Schottky junctions inside composites are highly beneficial for gas sensor activities. Jun et al. synthesized the heterostructures of  $\text{Ti}_3\text{C}_2\text{T}_x$  MXene and poly (3,4 ethylenedioxythiophene) polystyrene sulfonate (PEDOT:PSS) using an in situ polymerization technique. The optimum heterostructure with 15%  $\text{Ti}_3\text{C}_2\text{T}_x$  MXene exhibited the best response of 36.7% to 100 ppm of  $\text{NH}_3$  gas with fast recovery (40 s) and response (117 s) times. From a comparison with previously researched  $\text{NH}_3$  sensors, they concluded that the direct charge transfers and chemisorption of oxygen play a crucial role in improving the sensing performance. In addition, the sensor displays a similar response signal regardless of the bending angles (240°, 180°, 120°, 60°), thereby representing its tremendous mechanical stability and potential to be utilized in wearable sensor devices, as indicated in Figure 10 [109].

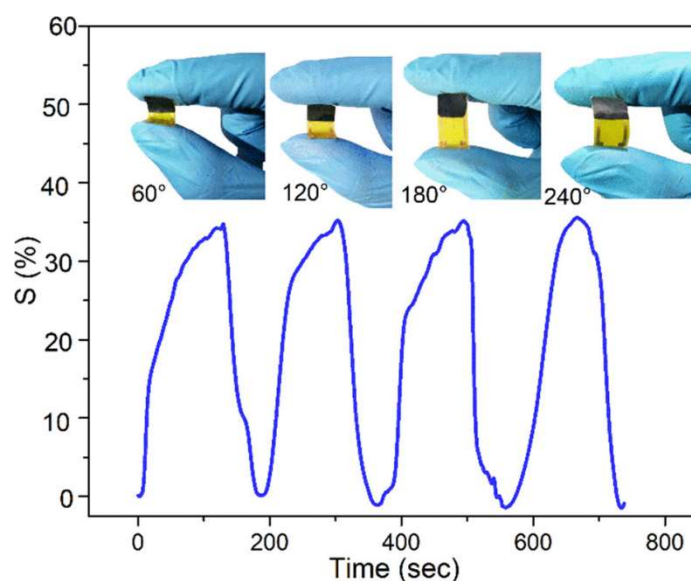


**Figure 10.** Gas-sensing signal of the as-prepared PEDOT:PSS/Ti<sub>3</sub>C<sub>2</sub>T<sub>x</sub> composite to 100 ppm NH<sub>3</sub> gas at a variety of bending angles (60°, 120°, 180°, 240°). Reprinted and adapted with permission from [109]. Copyright 2020 American Chemical Society.

Wang et al. [9] prepared nanocomposites of PEDOT:PSS/Ti<sub>3</sub>C<sub>2</sub>T<sub>x</sub> MXene for a methanol sensor at room temperature. A gas sensor based on the composite with a mass ratio of 4:1 (Ti<sub>3</sub>C<sub>2</sub>T<sub>x</sub> MXene 20 wt%) revealed the highest response (5.5%) to 300 ppm methanol compared to pure PEDOT:PSS (4.67%) and pristine Ti<sub>3</sub>C<sub>2</sub>T<sub>x</sub> MXene (1.13%) [9]. The presence of Ti<sub>3</sub>C<sub>2</sub>T<sub>x</sub> in the polymer matrix enlarges the interchain space of PEDOT:PSS, making electron hopping difficult. The high metallic behavior enables the composite sensors to run under 0.1 V with low power consumption. The formation of heterojunctions at the interfaces of the conductive polymers and Ti<sub>3</sub>C<sub>2</sub>T<sub>x</sub> MXene significantly improves the mechanical flexibility and practicality of wearable gas sensors.

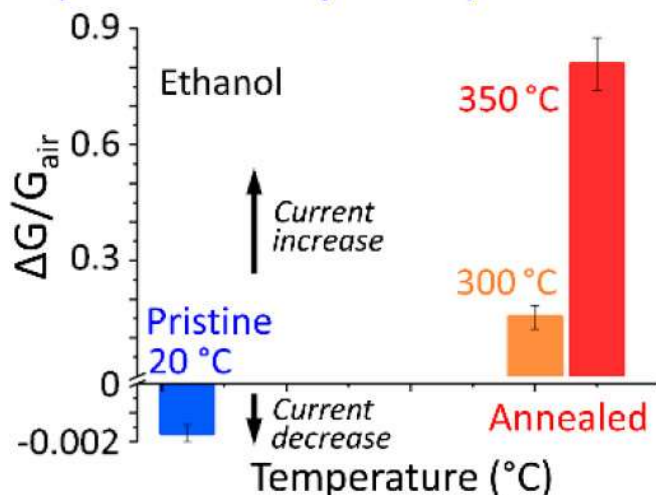
#### 4.3. MXene-Semiconductive Metal Oxide Composites

Metal oxide semiconductors (MOS) are the most used gas-sensing materials for a variety of applications because of their facile synthesis, high sensitivity, and easy functionalization. However, the high working temperature and low selectivity were the main disadvantages of these MOS-based gas sensors. To solve this dilemma, a combination of metallic Ti<sub>3</sub>C<sub>2</sub>T<sub>x</sub> MXene and semiconducting MOS can overcome the low selectivity and high operating temperature issues. The formation of the Schottky junction at the interfaces of the metal oxide semiconductor and Ti<sub>3</sub>C<sub>2</sub>T<sub>x</sub> MXene can accelerate the movement of only one type of charge carriers across the interface.

There are several extensive reports on the gas-sensing activities of MOS/MXene heterostructures, where MXenes are a conductive layer and MOS is the main sensing material [127–130]. Ta et al. [131] constructed a ZnO/Ti<sub>3</sub>C<sub>2</sub>T<sub>x</sub> MXene heterostructure, which consists of 1D ZnO nanoparticles and 2D few-layered Ti<sub>3</sub>C<sub>2</sub>T<sub>x</sub> MXene, using a simple technique. The optimized heterostructure exhibited responses of 54% and 25% to 10 and 5 ppm of NO<sub>2</sub>, respectively. Partially oxidized TiO<sub>2</sub>/Ti<sub>3</sub>C<sub>2</sub>T<sub>x</sub> composites were synthesized by oxygen plasma treatment at 350 °C, substantially increasing the responses to acetone (180% at 2000 ppb) and ethanol (22.5% at 100 ppm) [132,133]. Ti<sub>3</sub>C<sub>2</sub>T<sub>x</sub> MXene is partially converted to TiO<sub>2</sub> nanoparticles, and the oxygen termination groups play a pivotal role in the enhancement of gas-sensing performance compared to the pure MXene, as shown in Figure 11.

## Annealing $Ti_3C_2T_x$ MXene sensors

(1) modified sensing behavior,  
improved sensitivity and response time:



(2) selective analyte recognition:

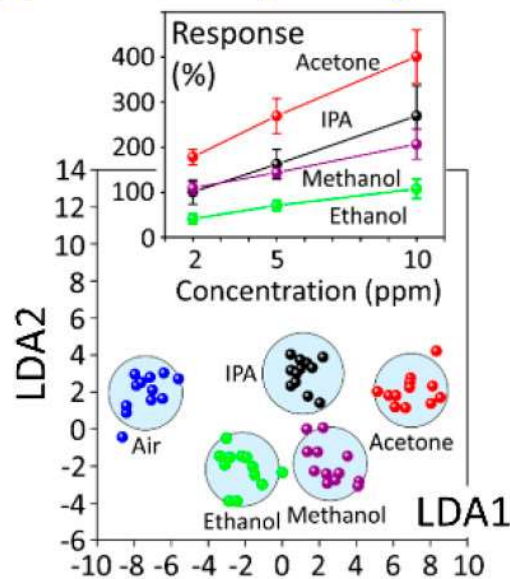
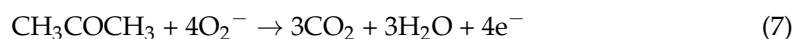
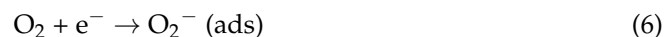


**Figure 11.** VOC-sensing activity of oxidized  $TiO_2/Ti_3C_2T_x$  composite. Reprinted and adapted with permission from [132]. Copyright 2020 American Chemical Society.

Wang et al. [8] synthesized a  $SnO-SnO_2/Ti_3C_2T_x$  composite for an acetone sensor at room temperature using the hydrothermal method. The creation of p-n junctions and Schottky junctions in the  $SnO-SnO_2/Ti_3C_2T_x$  composite was key to improving the acetone-sensing responses ( $R_g/R_a = 12.1$ , 100 ppm), which were 11 and 4 times higher than those of pure  $Ti_3C_2T_x$  and  $SnO-SnO_2$ , respectively. After the connection, the electron moved from the n-type  $SnO_2$  and metallic  $Ti_3C_2T_x$  to the p-type  $SnO$  because of the differences in Fermi energy; the electron depletion layer (EDL) decreases when acetone enters. Therefore, the resistance of the sensing material increased, and the oxidation-reaction mechanism of the entire process can be explained as



Bimetallic oxide is also available for gas sensing because it has several oxygen vacancies. Zou et al. [115] prepared a  $Fe_2(MoO_4)_3/Ti_3C_2T_x$  MXene heterostructure using a hydrothermal method and sensed 100 ppm of n-butanol at 120 °C (response = 43.1%). The nanocomposite showed a large specific surface area ( $47 \text{ m}^2/\text{g}$ ) with a small pore size (10 nm), which was better than that of pure  $Fe_2(MoO_4)_3$  ( $11 \text{ m}^2/\text{g}$ , 20.8 nm). The composite with 1 wt% of  $Ti_3C_2T_x$  MXene showed a small pore size caused by nanoparticles blocking the hole. Rich active sites and abundant chemical oxygen species were the main factors for enhancing the gas-sensing performance with a short response time (18 s).

#### 4.4. Self-Powered Gas Sensors

Gas sensors require external power sources, which restricts their application in wearable devices. Several researchers focused on self-powered gas sensors to tackle this problem. Zhang et al. [104] studied a  $Co_3O_4/Ti_3C_2T_x$  composite-based gas sensor, which was driven by the  $ZnO/Ti_3C_2T_x$  nanostructure array piezoelectric nanogenerator (PENG) using the titanium and aluminum foils as electrodes.  $ZnO/Ti_3C_2T_x$  nanowires on the Ti foil acted as the power source, converting the mechanical energy of human movement into electrical energy. The power generated from PENG could run the gas sensor device, which

exhibited high sensitivity ( $R_g/R_a = 9.2$ ) to 10 ppm of HCHO with a fast recovery speed (recovery time = 5 s) [104].

Wang et al. [134] studied CuO/Ti<sub>3</sub>C<sub>2</sub>T<sub>x</sub> composites for a self-powered NH<sub>3</sub> sensor at room temperature. The sensor was driven by a triboelectric nanogenerator (TEMG) using latex and polytetrafluoroethylene (PTFE). The resistance of the CuO/Ti<sub>3</sub>C<sub>2</sub>T<sub>x</sub> composite increased when exposed to NH<sub>3</sub> gas (0–100 ppm) which resulted in a voltage–resistance (U–R) curve through the load, as shown in Figure 12. The output voltage versus gas concentration curves can be obtained via sensing signals, and then can be converted to resistance versus gas concentration curves using the corresponding U–R relationship. The CuO/Ti<sub>3</sub>C<sub>2</sub>T<sub>x</sub> composite showed a good response (25%) to 100 ppm of NH<sub>3</sub> and could detect the deterioration of pork because it releases NH<sub>3</sub> as it rots. Here, CuO showed p-type semiconductor behavior with holes as the majority carriers; the hole concentration increased when it was in contact with oxygen molecules. Many electrons jump into the conduction band of CuO under exposure to an NH<sub>3</sub> atmosphere, and this increases the resistance of CuO. In the same context, the resistance of organ-like MXene increased in an NH<sub>3</sub> environment. The excellent interaction between negatively charged MXene and positively charged CuO led to an effective combination for improved NH<sub>3</sub> sensing. A wearable TEMG device had a short-circuit current of 34  $\mu$ A (open-circuit voltage = 810 V) and could light 480 LEDs with a power density of 10.8 W·m<sup>-2</sup>.

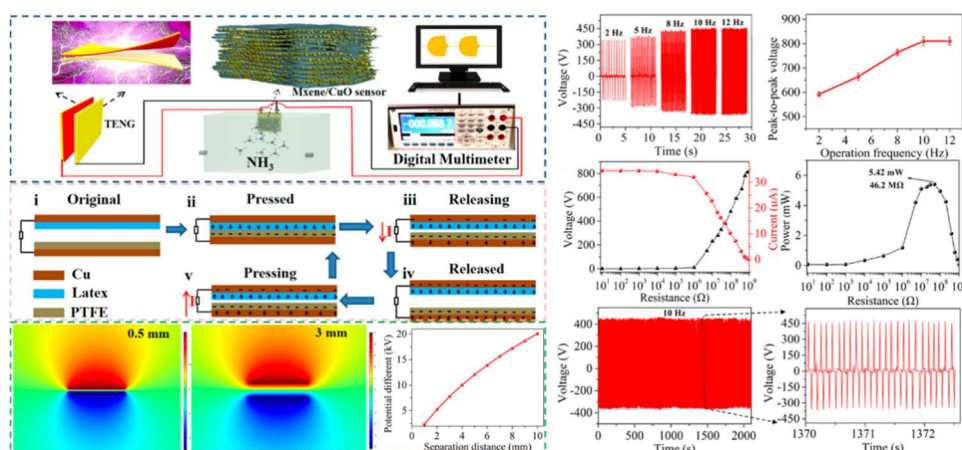
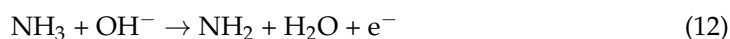


**Figure 12.** Schematic and experimental results of a self-powered ammonia sensor driven by TEMG. Reprinted and adapted with permission from [134]. Copyright 2021 American Chemical Society.

Self-powered composites may be essential in the fields of Internet of Things (IoT) and flexible devices. In this regard, CuO/Ti<sub>3</sub>C<sub>2</sub>T<sub>x</sub> composites have the potential to be integrated into wearable sensors powered by human motion. The improved chemiresistive gas sensor mechanisms can be explained by



## 5. Applications of $Ti_3C_2T_x$ MXene for Energy Harvesting

### 5.1. MXene in Triboelectric Energy

Mechanical energy is converted into useful electrical energy through triboelectrification and electrostatic induction. This phenomenon, commonly observed in our everyday lives, causes random electrostatic charges. When two materials with different electron affinities come into continuous contact and separate, they become oppositely charged through contact electrification, which causes a transfer of electrons from one material surface to another [135,136]. Wang et al. [137] proposed an energy harvesting technique that provides a new approach for producing electricity through frictional energy such as body movements, ocean waves, and mechanical vibrations. The efficiency of power generation depends on the difference in the electron affinity of materials. Material pairs with large electron affinity differences are preferred over materials with poor electron affinities [138]. Most triboelectric devices work on four principal modes: contact-separation, lateral sliding, freestanding, and single electrode modes.

MXenes play a crucial role here because of their unique properties such as high surface area, electrical conductivity, and tunable electronegativity, which make  $Ti_3C_2T_x$  MXenes a suitable candidate for this approach to energy harvesting. Poly (tetrafluoroethylene) PTFE and fluorinated ethylene propylene (FEP) are the most used as negative friction layers; however, they exhibit poor conductivity. Dong et al. [139] reported the use of  $Ti_3C_2T_x$  MXenes as active electronegative material triboelectric nanogenerators (TEENG) for generating high output powers, where  $Ti_3C_2T_x$  MXenes were considered to be as good as PTFE with the PET-ITO electrode (Figure 13) [139–141].

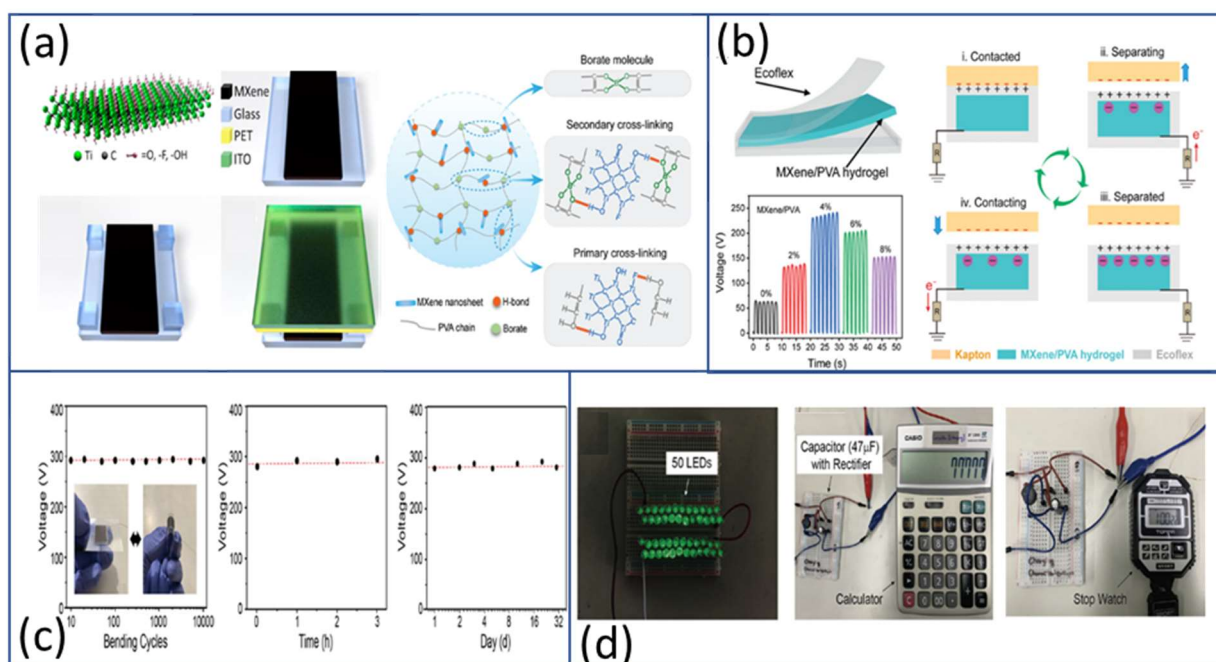


**Figure 13.** (a) Structure of  $Ti_3C_2T_x$  MXene and MXene triboelectric nanogenerator (MXene TENG) assembled as shown in the schematics. (b) MXene/PVA hydrogel flexible multifunctional TENG. (c) Mechanical stability and reliability of EAPs-based TENG with diverse applications. (d) The 50 LEDs, calculator, and stopwatch were powered by the TENG. Reprinted and adapted with permission from [139,142–144].

Further, MXenes can be used as nanofillers in other materials to improve mechanical, physical, and surface properties. The incorporation of only 4%  $Ti_3C_2T_x$  MXenes into a PVA (polyvinyl alcohol) hydrogel improves conductivity as well as the maximum output voltage of 230 V and output current of 270 nA [142,143]. This system is effectively used for self-recognizing handwriting systems with great sensitivity, reliability, and identifiability

as a self-powered sensor. Moreover, MXene-based materials are being studied for use in wearable flexible devices. For example, a stretchable and shape-adaptive TENG system with MXenes and liquid metal electrodes was proposed to drive wearable electronics with open-circuit voltages of 300 V [143]. Overall, the combination of  $\text{Ti}_3\text{C}_2\text{T}_x$  MXene and liquid metal led to excellent fluidity and high electronegativity.

Further, a self-powered 3D-printed smart glove with a  $\text{Ti}_3\text{C}_2\text{T}_x$  MXene/ecoflex nanocomposite was developed for gaming and human-machine interfaces. Adding MXenes into the ecoflex led to high charge density, ultraflexibility, high output TENG performance, and wide pressure detection range (0–120 kPa). Interestingly,  $\text{Ti}_3\text{C}_2\text{T}_x$  MXenes flakes with added polymer matrices displayed a superior charge retention capability and highly sustainable wearable TENG [144], which led to its application for operating small portable electronic devices such as LEDs, a calculator, and a stopwatch.  $\text{Ti}_3\text{C}_2\text{T}_x$  MXene-based nanocomposites also realized a high dielectric constant and high surface charge density in the poly(vinylidene fluoride-tetrafluoroethylene) PVDF-TrFE polymer matrix [145]. The maximum power obtained was  $4.02 \text{ W/m}^2$  under a  $4 \text{ M}\Omega$  external resistance.

### 5.2. MXene in Piezoelectric Energy Harvesting

Piezoelectric energy harvesting is a relatively new technique for converting mechanical energy into electricity. Its simple manufacturing process makes it ideal for harvesting energy and powering small-scale devices. Various materials show piezoelectric effects in response to applied mechanical stress such as semiconductors, ceramics, and polymers. When external force is applied to a piezoelectric material, the dipole moment of the material changes and leads to imbalance at the two poles. The crystal lattice consists of ions with asymmetric charges or molecular groups, and it is responsible for this dipole moment. A typical example of piezoelectricity is the wurtzite structure of the ZnO crystal lattice. The generated charge is collected by charge-collector materials. There is no dipole moment on the ZnO crystal lattice when there is no external force because the two charge centers of anion and cations cancel each other. This original state becomes disturbed through compression or stretching with external force, which separates the cation and anion charge centers. This is how the piezoelectric potential is generated and induces the flow of free electrons through the external circuit to attain a new equilibrium state.

Tan et al. [146] reported the piezoelectricity of 2D  $\text{Ti}_3\text{C}_2\text{T}_x$  MXene in monolayer and multilayer structures with a low band gap. They revealed that the generation of continuous piezoelectric potential occurs in the direction of the armchair at an atomic structure level. The double-layer structure does not have a piezoelectric polarization phenomenon because the same and opposite polarization can cancel or superimpose each other. However, in the monolayer  $\text{Ti}_3\text{C}_2\text{T}_x$  MXene, an inverse piezoelectric effect is inevitable. Li-doped ZnO nanowires grown on MXenes result in the performance enhancement of PENG, where MXenes ( $\text{Ti}_3\text{C}_2\text{T}_x$ ) served as ground for the more effective polarization of Li-doped ZnO [147], as shown in Figure 14.

Han et al. [148] designed an anisotropic PVDF/MXene device with directionally oriented foam as the directional sensor and claimed to have a highest sensitivity of  $41.3 \text{ nA/kPa}$ , which outperforms the other polymer-based piezoelectric sensors. Other reports showed that the incorporation of  $\text{Ti}_3\text{C}_2\text{T}_x$  MXene into the polymer matrix of PVDF enhances the  $\beta$ -phase, which directly affects the output piezoelectric performance [140]. Ma et al. [149] introduced a highly flexible piezoelectric sensor with the qualities of greatly changed interlayer distance under external pressure, high sensitivity, and a fast response up to 30 s. This  $\text{Ti}_3\text{C}_2\text{T}_x$  MXene-based piezoelectric sensor could also detect human activities with extraordinarily reversible compressibility.

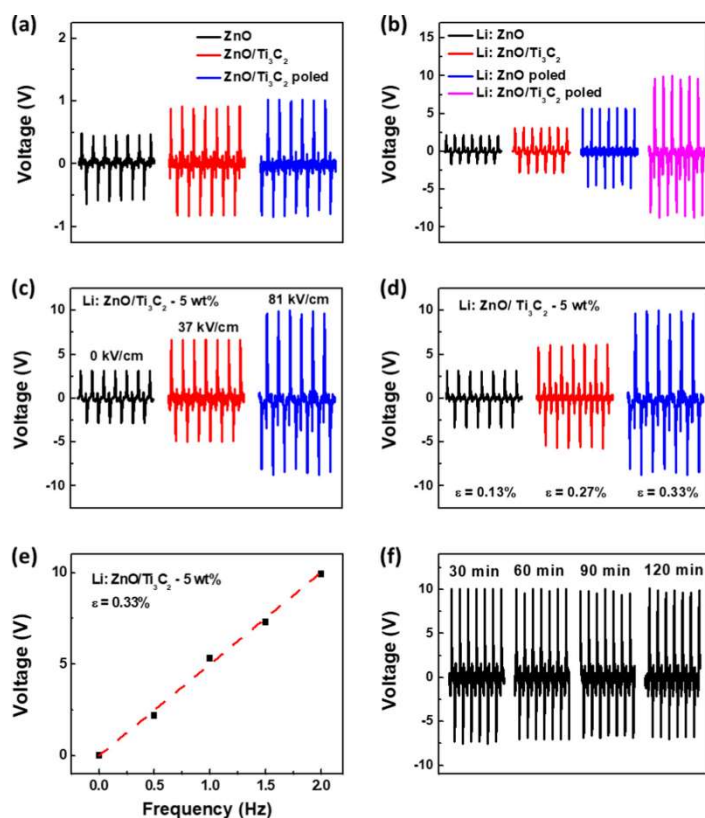


**Figure 14.** (a–f) Output performance of PENG fabricated with Li:ZnO/Ti<sub>3</sub>C<sub>2</sub>T<sub>x</sub> composites. Reprinted and adapted with permission from [147]. Copyright 2022 American Chemical Society.

### 5.3. MXene in Thermoelectric Energy Harvesting

This method involves directly converting heat into electricity using Ti<sub>3</sub>C<sub>2</sub>T<sub>x</sub> MXenes as both bulk and additives in thermoelectric energy harvesting applications. The temperature gradient induced in the device resulted in the diffusion of charged carriers from the hot side to the cold side. One side of the n-type and p-type junction absorbs heat and the other side releases heat when a current is applied to the device. This utilizes energy harvesting and cooling applications without the use of moving parts. Here, Ti<sub>3</sub>C<sub>2</sub>T<sub>x</sub> MXenes are promising candidates for thermoelectric materials because of their unique electronic structure.

Chang et al. [150] studied the thermoelectric properties of MXenes (ScYCT<sub>2</sub>) and showed that MXene structures have high thermoelectric properties. The n-type (ScYC(OH)<sub>2</sub>) showed a maximum power factor of 0.072 W/mK<sup>2</sup> at 900 K and a ZT value exceeding 3 and superior electron transfer properties. Further, the thermoelectric properties of Ti<sub>3</sub>C<sub>2</sub>T<sub>x</sub> MXene and its energy conversion efficiency can be improved effectively by surface modifications [151]. The addition of Ti<sub>3</sub>C<sub>2</sub>T<sub>x</sub> MXene to the SWCNT film improved the thermoelectric conversion efficiency by 25 times because of its diverse electronic properties [143]. The heterostructure of Ti<sub>3</sub>C<sub>2</sub>T<sub>x</sub>MXene helped enhance the Seebeck coefficient up to  $-32.2 \mu\text{V K}^{-1}$ .

### 5.4. MXene for Hydroelectric Energy Harvesting

Ti<sub>3</sub>C<sub>2</sub>T<sub>x</sub> MXenes are known to harvest hydroelectric energy because of their hydrophilic, high surface area, and three-dimensional (3D) nanosheet structure. Humidity is abundantly available in nature and can be used to harvest clean energy from the environment. Through water vapor pressure, the water molecules adsorb into the micro/nanochannels inside the material of interest and result in an electric charge transfer by creating a ionic concentration gradient inside the material.

Owing to this ionic dissociation of the hydrophilic functional group, the free protons (H<sup>+</sup>) or mobile charges move along the concentration gradient until it reaches its maximum value. This gradient disappears when the moisture supply is cut off [138,139]. Further,

the largely functionalized surface group is a more active material for hydroelectric energy harvesting, therefore, MXenes are suitable materials for hydroelectric energy harvesting because of their availability to functionalized surface groups (-F, -OH, etc.). The porous structure of  $\text{Ti}_3\text{C}_2\text{T}_x$  MXene promotes the transport of water molecules [152]. Recently, the  $\text{Ti}_3\text{C}_2\text{T}_x$  aerogel was used as a moisture-driven energy harvester for electric power generation [153]. The 3D-structured bilayer of  $\text{Ti}_3\text{C}_2\text{T}_x$  MXene with a PAN aerogel resulted in high-output electric energy with a sustained voltage of around 430 mV in a wide range of humidity. The presence of abundant ions such as  $\text{Ca}^{2+}$  and  $\text{Cl}^-$  ions helps facilitate the large moisture gradient. In addition,  $\text{Ti}_3\text{C}_2\text{T}_x$  MXenes were discovered to be good for transpiration-driven power generators using water and electrolyte solutions [154]. This was also used to charge a battery with a power density of  $24.8 \mu\text{W cm}^{-2}$ . Li et al. [155] studied  $\text{Ti}_3\text{C}_2\text{T}_x$  MXene-based composite membranes with directional proton diffusion to generate electricity with moisture stimuli. Here, a multifunctional soft actuator was developed, as shown in Figure 15.

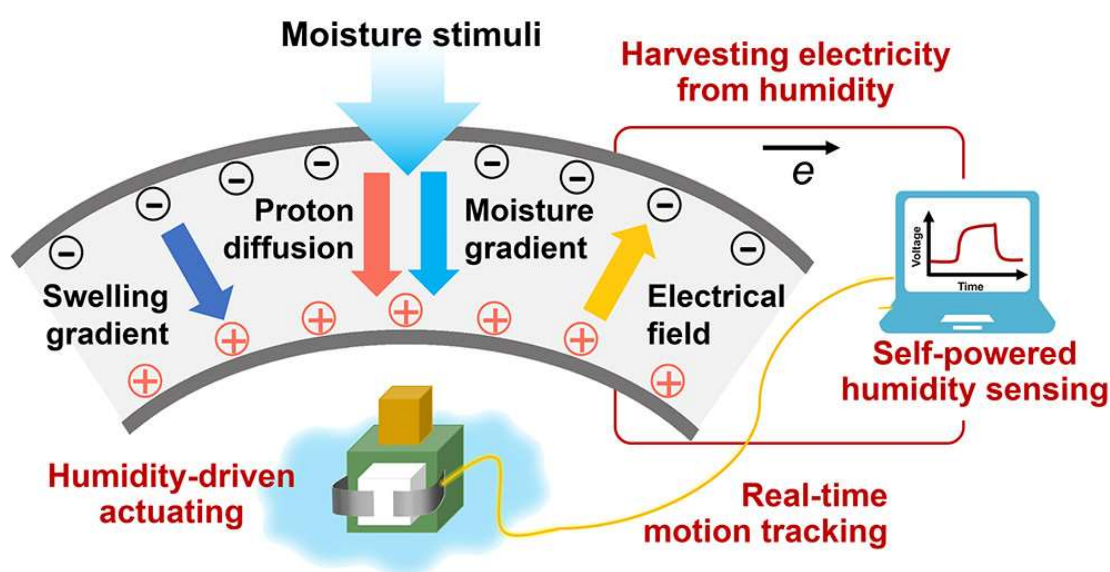


**Figure 15.** MXene for harvesting energy with moisture stimuli. Reprinted and adapted with permission from [155]. Copyright 2021 American Chemical Society.

### 5.5. MXene for Solar Energy Harvesting

MXenes have great potential as a future material in solar cells. The continuous improvement in solar cell systems is expected to replace conventional materials with 2D materials. Two-dimensional semiconductor materials such as graphene, transition-metal dichalcogenide, and black phosphorous are potential candidates for making next-generation ultrathin solar cells. Recently, perovskite solar cells (PSCs) with perovskite crystal structures were highly studied for their quick energy conversion efficiencies [156]. The distortions in the crystallographic phase transition in the perovskite crystal structure were induced by varying temperature from the cubic to the tetragonal phase.  $\text{Ti}_3\text{C}_2\text{T}_x$  MXenes have also been used as additives in PSCs to overcome the potential challenges with PSCs, including their high instability upon exposure to air.  $\text{Ti}_3\text{C}_2\text{T}_x$  MXene has also been used to enhance carrier mobility and to improve the performance of PSCs by retarding the crystallization rate [157]. The charge transfer is facilitated through high electrical conductivity and the mobility of  $\text{Ti}_3\text{C}_2\text{T}_x$  MXenes. Further, the addition of  $\text{Ti}_3\text{C}_2\text{T}_x$  MXene in the perovskite film can shift the work function [149]. Zheng et al. [158] showed the quality-controlling ability of  $\text{SiO}_2/\text{Ti}_3\text{C}_2\text{T}_x$  MXene in a perovskite film with defect density, crystal size, etc. Similarly, interfacial defects are reduced with the addition of  $\text{Ti}_3\text{C}_2\text{T}_x$  QDs (TQDs), and they improve the carrier mobility of perovskite film (Figure 16) [156,159].

Thus,  $\text{Ti}_3\text{C}_2\text{T}_x$  MXene has the potential to be used as an additive in perovskite film and improve the performance of devices.

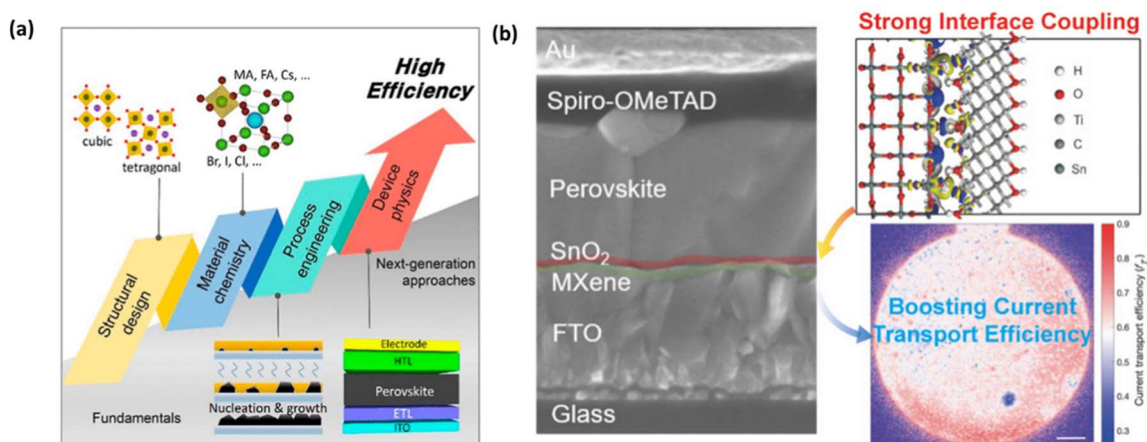


**Figure 16.** (a) Perovskite solar cell, (b) Interface boosting charge transport. Reprinted and adapted with permission from [156,159]. Copyright 2020 American Chemical Society.

$\text{Ti}_3\text{C}_2\text{T}_x$  MXene is also used as a flexible electrode material in organic solar cells (OSCs). OSCs are promising technologies for wearable and super flexible future electronics because of their qualities such as flexibility, light weight, and portability. Although the indium tin-oxide (ITO) electrode is used because of its high conductivity and transparency, ITO-based electrodes need to be replaced with other flexible electrodes when developing ultraflexible wearable electronic devices. Nirmal et al. [160] introduced a multilayer  $\text{Ti}_3\text{C}_2\text{T}_x$  MXene/Ag/MXene structure as a flexible electrode with sustained photovoltaic performance and memory retention functionalities. This device showed reliable resistive switching behavior at low operating voltages of 0.60 and  $-0.33$  V, and stable endurance performance ( $4 \times 10^3$ ). Further, a  $\text{Ti}_3\text{C}_2\text{T}_x$  MXene/Ag NWs/ colorless polyimide hybrid electrode with high conductivity was fabricated with considerably lower sheet resistance ( $13.08 \text{ Ohm sq}^{-1}$ ) [160,161]. The designed CuSe/ $\text{Ti}_3\text{C}_2\text{T}_x$  CE counter electrode showed excellent electrocatalytic activity towards polysulfide redox reactions because of its unique three-dimensional structure. Further,  $\text{Ti}_3\text{C}_2\text{T}_x$  MXene when added to a zinc oxide (ZnO) precursor can also be utilized in the electron transport layer (ETL) [161,162]. The optimized concentration of  $\text{Ti}_3\text{C}_2\text{T}_x$  with 0.5 and 2 wt% in the ETL exhibited power conversion efficiencies of 14.1% and 13.7%, respectively. The addition of MXene materials is a promising approach for improving the efficiency and stability of OSCs.

## 6. Conclusions and Outlook

The review summarized the synthesis and applications of  $\text{Ti}_3\text{C}_2\text{T}_x$  MXenes and their composites for toxic gas sensors. A brief review of MXene-based energy harvesting from various ambient sources was also provided, including thermoelectric energy, piezoelectric and triboelectric energy, hydroelectric energy, and solar energy. The effects of etching techniques (HF etching, HF-free etching), intercalation, and exfoliation on the morphology and structure of MXenes was examined. However, the review focused on HF etching because it is well-established and easy to use.

The hydrophilicity, surface tunability, high electrical conductivity, high surface area, and good optical transmittance of  $\text{Ti}_3\text{C}_2\text{T}_x$  MXenes provide a tremendous opportunity for these materials to be utilized in various areas of gas sensors and energy harvesting for realizing advanced device performances. The high electrical conductivity and rich surface termination groups may be the key features of  $\text{Ti}_3\text{C}_2\text{T}_x$  MXene for applications in those fields. The hybridization of  $\text{Ti}_3\text{C}_2\text{T}_x$  MXene with other materials to form functional composites is a good strategy to boost performance to an even higher level. Although

the proposed mechanisms of gas adsorption and the resulting electron transport remain debatable, we are indeed moving closer toward filling the gaps between known facts.

More MXenes and MXene-based composites must be explored in future to find their unparalleled qualities and expand their breadth of applications. Gas sensors are expected to become one of the key sectors that need these advanced nanomaterials.

**Author Contributions:** Conceptualization, methodology, validation, formal analysis, investigation, resources, data curation, Q.T.H.T.; writing—original draft preparation, D.T.; writing—review and editing, visualization, supervision, project administration, funding acquisition, J.-S.N. All authors have read and agreed to the published version of the manuscript.

**Funding:** This research was funded by a National Research Foundation of Korea (NRF) grant funded by the Korean government (MSIT) (No. 2019R1A2C1008746).

**Institutional Review Board Statement:** Not applicable.

**Informed Consent Statement:** Not applicable.

**Data Availability Statement:** Not applicable.

**Conflicts of Interest:** The authors declare no conflict of interest.

## References

1. Cristoloveanu, S.; Wan, J.; Zaslavsky, A. A Review of Sharp-Switching Devices for Ultra-Low Power Applications. *IEEE J. Electron Devices Soc.* **2016**, *4*, 215–226. [[CrossRef](#)]
2. Raza, U.; Kulkarni, P.; Sooriyabandara, M. Low Power Wide Area Networks: An Overview. *IEEE Commun. Surv. Tutor.* **2017**, *19*, 855–873. [[CrossRef](#)]
3. Nazir, G.; Rehman, A.; Park, S.-J. Energy-Efficient Tunneling Field-Effect Transistors for Low-Power Device Applications: Challenges and Opportunities. *ACS Appl. Mater. Interfaces* **2020**, *12*, 47127–47163. [[CrossRef](#)] [[PubMed](#)]
4. Novoselov, K.S.; Geim, A.K.; Morozov, S.V.; Jiang, D.; Zhang, Y.; Dubonos, S.V.; Grigorieva, I.V.; Firsov, A.A. Electric Field Effect in Atomically Thin Carbon Films. *Science* **2004**, *306*, 666–669. [[CrossRef](#)] [[PubMed](#)]
5. Alhabeab, M.; Maleski, K.; Anasori, B.; Lelyukh, P.; Clark, L.; Sin, S.; Gogotsi, Y. Guidelines for Synthesis and Processing of Two-Dimensional Titanium Carbide ( $\text{Ti}_3\text{C}_2\text{T}_x$  MXene). *Chem. Mater.* **2017**, *29*, 7633–7644. [[CrossRef](#)]
6. Zhang, H.-F.; Xuan, J.-Y.; Zhang, Q.; Sun, M.-L.; Jia, F.-C.; Wang, X.-M.; Yin, G.-C.; Lu, S.-Y. Strategies and Challenges for Enhancing Performance of MXene-Based Gas Sensors: A Review. *Rare Met.* **2022**, *41*, 3976–3999.
7. Hong, L.; Guo, R.; Yuan, Y.; Ji, X.; Li, Z.; Lin, Z.; Pan, W. Recent Progress of Two-Dimensional MXenes in Photocatalytic Applications: A Review. *Mater. Today Energy* **2020**, *18*, 100521. [[CrossRef](#)]
8. Wang, Z.; Wang, F.; Hermawan, A.; Asakura, Y.; Hasegawa, T.; Kumagai, H.; Kato, H.; Kakihana, M.; Zhu, J.; Yin, S. SnO-SnO<sub>2</sub> Modified Two-Dimensional MXene  $\text{Ti}_3\text{C}_2\text{T}_x$  for Acetone Gas Sensor Working at Room Temperature. *J. Mater. Sci. Technol.* **2021**, *73*, 128–138. [[CrossRef](#)]
9. Wang, X.; Sun, K.; Li, K.; Li, X.; Gogotsi, Y.  $\text{Ti}_3\text{C}_2\text{T}_x$ /PEDOT: PSS Hybrid Materials for Room-Temperature Methanol Sensor. *Chin. Chem. Lett.* **2020**, *31*, 1018–1021. [[CrossRef](#)]
10. Naguib, M.; Kurtoglu, M.; Presser, V.; Lu, J.; Niu, J.; Heon, M.; Hultman, L.; Gogotsi, Y.; Barsoum, M.W. Two-Dimensional Nanocrystals Produced by Exfoliation of  $\text{Ti}_3\text{AlC}_2$ . *Adv. Mater.* **2011**, *23*, 4248–4253. [[CrossRef](#)]
11. Tran, N.M.; Ta, Q.T.H.; Noh, J.-S. Unusual Synthesis of Safflower-Shaped  $\text{TiO}_2/\text{Ti}_3\text{C}_2$  Heterostructures Initiated from Two-Dimensional  $\text{Ti}_3\text{C}_2$  MXene. *Appl. Surf. Sci.* **2021**, *538*, 148023. [[CrossRef](#)]
12. Sreedhar, A.; Ta, Q.T.H.; Noh, J.-S. 2D  $\text{Ti}_3\text{C}_2$  MXene Interfaced ZnO/ $\text{WO}_3$  Thin Film Nanostructures towards Improved Photoelectrochemical Water Splitting. *J. Electroanal. Chem.* **2023**, *940*, 117509. [[CrossRef](#)]
13. My Tran, N.; Thanh Hoai Ta, Q.; Sreedhar, A.; Noh, J.S.  $\text{Ti}_3\text{C}_2\text{T}_x$  MXene Playing as a Strong Methylene Blue Adsorbent in Wastewater. *Appl. Surf. Sci.* **2021**, *537*, 148006. [[CrossRef](#)]
14. Nguyen, V.-H.; Nguyen, B.-S.; Hu, C.; Nguyen, C.C.; Nguyen, D.L.T.; Nguyen Dinh, M.T.; Vo, D.-V.N.; Trinh, Q.T.; Shokouhimehr, M.; Hasani, A. Novel Architecture Titanium Carbide ( $\text{Ti}_3\text{C}_2\text{T}_x$ ) MXene Cocatalysts toward Photocatalytic Hydrogen Production: A Mini-Review. *Nanomaterials* **2020**, *10*, 602. [[CrossRef](#)] [[PubMed](#)]
15. Mohammadi, A.V.; Rosen, J.; Gogotsi, Y. The World of Two-Dimensional Carbides and Nitrides (MXenes). *Science* **2021**, *372*, eabf1581. [[CrossRef](#)]
16. Li, Q.; Li, Y.; Zeng, W. Preparation and Application of 2D MXene-Based Gas Sensors: A Review. *Chemosensors* **2021**, *9*, 225. [[CrossRef](#)]
17. Wu, Z.; Shen, J.; Li, C.; Zhang, C.; Feng, K.; Wang, Z.; Wang, X.; Meira, D.M.; Cai, M.; Zhang, D.  $\text{Mo}_2\text{TiC}_2$  MXene-Supported Ru Clusters for Efficient Photothermal Reverse Water–Gas Shift. *ACS Nano* **2022**, *17*, 1550–1559. [[CrossRef](#)]

18. Gandla, D.; Zhang, F.; Tan, D.Q. Advantage of Larger Interlayer Spacing of a  $\text{Mo}_2\text{Ti}_2\text{C}_3$  MXene Free-Standing Film Electrode toward an Excellent Performance Supercapacitor in a Binary Ionic Liquid–Organic Electrolyte. *ACS Omega* **2022**, *7*, 7190–7198. [[CrossRef](#)]
19. Tran, V.A.; Tran, N.T.; Doan, V.D.; Nguyen, T.-Q.; Thi, H.H.P.; Vo, G.N.L. Application Prospects of MXenes Materials Modifications for Sensors. *Micromachines* **2023**, *14*, 247. [[CrossRef](#)]
20. Ji, H.; Zeng, W.; Li, Y. Gas Sensing Mechanisms of Metal Oxide Semiconductors: A Focus Review. *Nanoscale* **2019**, *11*, 22664–22684. [[CrossRef](#)]
21. Ta, Q.T.H.; Tran, N.M.; Tri, N.N.; Sreedhar, A.; Noh, J.S. Highly Surface-Active Si-Doped  $\text{TiO}_2/\text{Ti}_3\text{C}_2\text{T}_x$  Heterostructure for Gas Sensing and Photodegradation of Toxic Matters. *Chem. Eng. J.* **2021**, *425*, 131437. [[CrossRef](#)]
22. Wu, M.; He, M.; Hu, Q.; Wu, Q.; Sun, G.; Xie, L.; Zhang, Z.; Zhu, Z.; Zhou, A.  $\text{Ti}_3\text{C}_2$  MXene-Based Sensors with High Selectivity for  $\text{NH}_3$  Detection at Room Temperature. *ACS Sens.* **2019**, *4*, 2763–2770. [[CrossRef](#)] [[PubMed](#)]
23. Ta, Q.T.H.; Tran, N.M.; Noh, J.-S. Rice Crust-Like  $\text{ZnO}/\text{Ti}_3\text{C}_2\text{T}_x$  MXene Hybrid Structures for Improved Photocatalytic Activity. *Catalysts* **2020**, *10*, 1140. [[CrossRef](#)]
24. Gogotsi, Y. *MXenes: From Discovery to Applications of Two-Dimensional Metal Carbides and Nitrides*; CRC Press: Boca Raton, FL, USA, 2023; ISBN 1000618943.
25. Bhati, V.S.; Kumar, M.; Banerjee, R. Gas Sensing Performance of 2D Nanomaterials/Metal Oxide Nanocomposites: A Review. *J. Mater. Chem. C* **2021**, *9*, 8776–8808. [[CrossRef](#)]
26. Cao, M.; Wang, F.; Wang, L.; Wu, W.; Lv, W.; Zhu, J. Room Temperature Oxidation of  $\text{Ti}_3\text{C}_2$  MXene for Supercapacitor Electrodes. *J. Electrochem. Soc.* **2017**, *164*, A3933–A3942. [[CrossRef](#)]
27. Cao, F.; Zhang, Y.; Wang, H.; Khan, K.; Tareen, A.K.; Qian, W.; Zhang, H.; Ågren, H. Recent Advances in Oxidation Stable Chemistry of 2D MXenes. *Adv. Mater.* **2022**, *34*, 2107554. [[CrossRef](#)] [[PubMed](#)]
28. Pei, Y.; Zhang, X.; Hui, Z.; Zhou, J.; Huang, X.; Sun, G.; Huang, W.  $\text{Ti}_3\text{C}_2\text{T}_x$  MXene for Sensing Applications: Recent Progress, Design Principles, and Future Perspectives. *ACS Nano* **2021**, *15*, 3996–4017. [[CrossRef](#)]
29. Zhang, H.; Li, M.; Zhu, C.; Tang, Q.; Kang, P.; Cao, J. Preparation of Magnetic  $\alpha\text{-Fe}_2\text{O}_3/\text{ZnFe}_2\text{O}_4@/\text{Ti}_3\text{C}_2$  MXene with Excellent Photocatalytic Performance. *Ceram. Int.* **2020**, *46*, 81–88. [[CrossRef](#)]
30. Shahzad, A.; Rasool, K.; Nawaz, M.; Miran, W.; Jang, J.; Moztahida, M.; Mahmoud, K.A.; Lee, D.S. Heterostructural  $\text{TiO}_2/\text{Ti}_3\text{C}_2\text{T}_x$  (MXene) for Photocatalytic Degradation of Antiepileptic Drug Carbamazepine. *Chem. Eng. J.* **2018**, *349*, 748–755. [[CrossRef](#)]
31. Thi, Q.V.; Han, J.; Park, J.; Kim, S.-S.; Jeon, D.-Y.; Joo, Y. Printable and Recyclable Carbon Nanotube Electronics with Degradable Soybean Oil-Based Polycationic Substrate as Gate Dielectrics. *Carbon* **2023**, *212*, 118089. [[CrossRef](#)]
32. Kim, S.J.; Koh, H.J.; Ren, C.E.; Kwon, O.; Maleski, K.; Cho, S.Y.; Anasori, B.; Kim, C.K.; Choi, Y.K.; Kim, J.; et al. Metallic  $\text{Ti}_3\text{C}_2\text{T}_x$  MXene Gas Sensors with Ultrahigh Signal-to-Noise Ratio. *ACS Nano* **2018**, *12*, 986–993. [[CrossRef](#)] [[PubMed](#)]
33. Solangi, N.H.; Mazari, S.A.; Mubarak, N.M.; Karri, R.R.; Rajamohan, N.; Vo, D.-V.N. Recent Trends in MXene-Based Material for Biomedical Applications. *Environ. Res.* **2023**, *222*, 115337. [[CrossRef](#)] [[PubMed](#)]
34. Hong, S.; Al Marzooqi, F.; El-Demellawi, J.K.; Al Marzooqi, N.; Arafat, H.A.; Alshareef, H.N. Ion-Selective Separation Using MXene-Based Membranes: A Review. *ACS Mater. Lett.* **2023**, *5*, 341–356. [[CrossRef](#)]
35. Verma, R.; Thakur, P.; Chauhan, A.; Jasrotia, R.; Thakur, A. A Review on MXene and Its' Composites for Electromagnetic Interference (EMI) Shielding Applications. *Carbon* **2023**, *208*, 170–190. [[CrossRef](#)]
36. Li, Y.; Huang, S.; Peng, S.; Jia, H.; Pang, J.; Ibarlucea, B.; Hou, C.; Cao, Y.; Zhou, W.; Liu, H. Toward Smart Sensing by MXene. *Small* **2023**, *19*, 2206126. [[CrossRef](#)] [[PubMed](#)]
37. Huang, W.-X.; Li, Z.-P.; Li, D.-D.; Hu, Z.-H.; Wu, C.; Lv, K.-L.; Li, Q.  $\text{Ti}_3\text{C}_2$  MXene: Recent Progress in Its Fundamentals, Synthesis, and Applications. *Rare Met.* **2022**, *41*, 3268–3300. [[CrossRef](#)]
38. Li, J.; Chen, X.; Zhu, X.; Jiang, Y.; Chang, X.; Sun, S. Two-Dimensional Transition Metal MXene-Based Gas Sensors: A Review. *Chinese Chem. Lett.* **2023**, 108286. [[CrossRef](#)]
39. Li, H.; Sun, B.; Gao, T.; Li, H.; Ren, Y.; Zhou, G.  $\text{Ti}_3\text{C}_2$  MXene Co-Catalyst Assembled with Mesoporous  $\text{TiO}_2$  for Boosting Photocatalytic Activity of Methyl Orange Degradation and Hydrogen Production. *Chin. J. Catal.* **2022**, *43*, 461–471. [[CrossRef](#)]
40. Barsoum, M.W.; Gogotsi, Y. Removing Roadblocks and Opening New Opportunities for MXenes. *Ceram. Int.* **2023**, *49*, 24112–24122. [[CrossRef](#)]
41. Simonenko, E.P.; Simonenko, N.P.; Mokrushin, A.S.; Simonenko, T.L.; Gorobtsov, P.Y.; Nagornov, I.A.; Korotcenkov, G.; Sysoev, V.V.; Kuznetsov, N.T. Application of Titanium Carbide MXenes in Chemiresistive Gas Sensors. *Nanomaterials* **2023**, *13*, 850. [[CrossRef](#)]
42. Khan, K.; Tareen, A.K.; Iqbal, M.; Ye, Z.; Xie, Z.; Mahmood, A.; Mahmood, N.; Zhang, H. Recent Progress in Emerging Novel MXenes Based Materials and Their Fascinating Sensing Applications. *Small* **2023**, *19*, e2206147. [[CrossRef](#)] [[PubMed](#)]
43. Janjhi, F.A.; Ihsanullah, I.; Bilal, M.; Castro-Muñoz, R.; Boczkaj, G.; Gallucci, F. MXene-Based Materials for Removal of Antibiotics and Heavy Metals from Wastewater—A Review. *Water Resour. Ind.* **2023**, *29*, 100202. [[CrossRef](#)]
44. Liu, X.; Li, M.; Zhang, Y.; Zhu, X.; Guan, Y. Self-Powered Wireless Sensor Node Based on RF Energy Harvesting and Management Combined Design. *Energy Convers. Manag.* **2023**, *292*, 117393. [[CrossRef](#)]
45. Miao, L.; Huo, Z.-M.; Rong, Y.; Mu, H.-W.; Sun, Z.-X. IoT Adaptive Threshold Energy Management Algorithm Based on Energy Harvesting. *Ad Hoc Netw.* **2023**, *149*, 103241. [[CrossRef](#)]

46. Su, Y.; Chen, S.; Liu, B.; Lu, H.; Luo, X.; Chen, C.; Li, W.; Long, Y.; Tai, H.; Xie, G. Maxwell Displacement Current Induced Wireless Self-Powered Gas Sensor Array. *Mater. Today Phys.* **2023**, *30*, 100951. [[CrossRef](#)]
47. Ghidui, M.; Lukatskaya, M.R.; Zhao, M.Q.; Gogotsi, Y.; Barsoum, M.W. Conductive Two-Dimensional Titanium Carbide “clay” with High Volumetric Capacitance. *Nature* **2015**, *516*, 78–81. [[CrossRef](#)] [[PubMed](#)]
48. Shuck, C.E.; Han, M.; Maleski, K.; Hantanasirisakul, K.; Kim, S.J.; Choi, J.; Reil, W.E.B.; Gogotsi, Y. Effect of  $Ti_3AlC_2$  MAX Phase on Structure and Properties of Resultant  $Ti_3C_2T_x$  MXene. *ACS Appl. Nano Mater.* **2019**, *2*, 3368–3376. [[CrossRef](#)]
49. Shahzad, F.; Alhabeab, M.; Hatter, C.B.; Anasori, B.; Hong, S.M.; Koo, C.M.; Gogotsi, Y. Electromagnetic Interference Shielding with 2D Transition Metal Carbides (MXenes). *Science* **2016**, *353*, 1137–1140. [[CrossRef](#)]
50. Cai, L.; Huang, Z.; Hu, W.; Hao, S.; Zhai, H.; Zhou, Y. Fabrication, Mechanical Properties, and Tribological Behaviors of  $Ti_2AlC$  and  $Ti_2AlSn_{0.2}C$  Solid Solutions. *J. Adv. Ceram.* **2017**, *6*, 90–99. [[CrossRef](#)]
51. Wang, X.; Mathis, T.S.; Li, K.; Lin, Z.; Vlcek, L.; Torita, T.; Osti, N.C.; Hatter, C.; Urbankowski, P.; Sarycheva, A.; et al. Influences from Solvents on Charge Storage in Titanium Carbide MXenes. *Nat. Energy* **2019**, *4*, 241–248. [[CrossRef](#)]
52. Uzun, S.; Seyedin, S.; Stoltzfus, A.L.; Levitt, A.S.; Alhabeab, M.; Anayee, M.; Strobel, C.J.; Razal, J.M.; Dion, G.; Gogotsi, Y. Knittable and Washable Multifunctional MXene-Coated Cellulose Yarns. *Adv. Funct. Mater.* **2019**, *29*, 1905015. [[CrossRef](#)]
53. Sreedhar, A.; Ta, Q.T.H.; Noh, J.-S. Role of Pn Junction Initiated Mixed-Dimensional 0D/2D, 1D/2D, and 2D/2D BiOX (X= Cl, Br, and I)/ $TiO_2$  Nanocomposite Interfaces for Environmental Remediation Applications: A Review. *Chemosphere* **2022**, *305*, 135478. [[CrossRef](#)]
54. Perera, A.; Madhushani, K.A.U.; Punchihewa, B.T.; Kumar, A.; Gupta, R.K. MXene-Based Nanomaterials for Multifunctional Applications. *Materials* **2023**, *16*, 1138. [[CrossRef](#)] [[PubMed](#)]
55. Nahiriak, S.; Ray, A.; Saruhan, B. Challenges and Future Prospects of the MXene-Based Materials for Energy Storage Applications. *Batteries* **2023**, *9*, 126. [[CrossRef](#)]
56. Li, Z.; Yu, L.; Milligan, C.; Ma, T.; Zhou, L.; Cui, Y.; Qi, Z.; Libretto, N.; Xu, B.; Luo, J.; et al. Two-Dimensional Transition Metal Carbides as Supports for Tuning the Chemistry of Catalytic Nanoparticles. *Nat. Commun.* **2018**, *9*, 5258. [[CrossRef](#)]
57. Naguib, M.; Mashtalir, O.; Carle, J.; Presser, V.; Lu, J.; Hultman, L.; Gogotsi, Y.; Barsoum, M.W. Two-Dimensional Transition Metal Carbides. *ACS Nano* **2012**, *6*, 1322–1331. [[CrossRef](#)]
58. Xiao, X.; Wang, H.; Urbankowski, P.; Gogotsi, Y. Topochemical Synthesis of 2D Materials. *Chem. Soc. Rev.* **2018**, *47*, 8744–8765. [[CrossRef](#)]
59. Shuck, C.E.; Gogotsi, Y. Taking MXenes from the Lab to Commercial Products. *Chem. Eng. J.* **2020**, *401*, 125786. [[CrossRef](#)]
60. Zhu, J.F.; Qi, G.Q.; Wang, F.; Yang, H.B. Synthesis of  $Ti_3AlC_2/Al_2O_3$  Nanopowders by Mechano-Chemical Reaction. *Adv. Powder Technol.* **2010**, *21*, 578–581. [[CrossRef](#)]
61. Wang, X.; Wu, L.; Gao, H.; Zhang, X. Synthesis of  $Ti_3AlC_2$  and electrochemical performance of  $Ti_3C_2T_x$  nanosheet electrode. *Sci. Sin. Chim.* **2018**, *48*, 289–297. [[CrossRef](#)]
62. Shahin, N.; Kazemi, S.; Heidarpour, A. Mechanochemical Synthesis Mechanism of  $Ti_3AlC_2$  MAX Phase from Elemental Powders of Ti, Al and C. *Adv. Powder Technol.* **2016**, *27*, 1775–1780. [[CrossRef](#)]
63. An, H.; Habib, T.; Shah, S.; Gao, H.; Radovic, M.; Green, M.J.; Lutkenhaus, J.L. Surface-Agnostic Highly Stretchable and Bendable Conductive MXene Multilayers. *Sci. Adv.* **2018**, *4*, eaaq0118. [[CrossRef](#)] [[PubMed](#)]
64. Jawaid, A.; Hassan, A.; Neher, G.; Nepal, D.; Pachter, R.; Kennedy, W.J.; Ramakrishnan, S.; Vaia, R.A. Halogen Etch of  $Ti_3AlC_2$  MAX Phase for MXene Fabrication. *ACS Nano* **2021**, *15*, 2771–2777.
65. Shi, H.; Zhang, P.; Liu, Z.; Park, S.; Lohe, M.R.; Wu, Y.; Shaygan Nia, A.; Yang, S.; Feng, X. Ambient-stable Two-dimensional Titanium Carbide (MXene) Enabled by Iodine Etching. *Angew. Chemie Int. Ed.* **2021**, *60*, 8689–8693.
66. Yang, S.; Zhang, P.; Wang, F.; Ricciardulli, A.G.; Lohe, M.R.; Blom, P.W.M.; Feng, X. Fluoride-free Synthesis of Two-dimensional Titanium Carbide (MXene) Using a Binary Aqueous System. *Angew. Chemie* **2018**, *130*, 15717–15721.
67. Li, T.; Yao, L.; Liu, Q.; Gu, J.; Luo, R.; Li, J.; Yan, X.; Wang, W.; Liu, P.; Chen, B. Fluorine-free Synthesis of High-purity  $Ti_3C_2T_x$  (T= OH, O) via Alkali Treatment. *Angew. Chemie Int. Ed.* **2018**, *57*, 6115–6119. [[CrossRef](#)] [[PubMed](#)]
68. Peng, W.; Kuai, Z.; Peng, J.; Guo, W.; Li, H.; Peng, C.; Chen, S. MXene-Based Gold Nanoparticle Catalyst with High Activity and Stability for 4-Nitrophenol Reduction. *J. Solid State Chem.* **2023**, *325*, 124166.
69. Hope, M.A.; Forse, A.C.; Griffith, K.J.; Lukatskaya, M.R.; Ghidui, M.; Gogotsi, Y.; Grey, C.P. NMR Reveals the Surface Functionalisation of  $Ti_3C_2$  MXene. *Phys. Chem. Chem. Phys.* **2016**, *18*, 5099–5102. [[CrossRef](#)]
70. Venkateshalu, S.; Grace, A.N. MXenes—A New Class of 2D Layered Materials: Synthesis, Properties, Applications as Supercapacitor Electrode and Beyond. *Appl. Mater. Today* **2020**, *18*, 100509.
71. Ding, L.; Wei, Y.; Li, L.; Zhang, T.; Wang, H.; Xue, J.; Ding, L.X.; Wang, S.; Caro, J.; Gogotsi, Y. MXene Molecular Sieving Membranes for Highly Efficient Gas Separation. *Nat. Commun.* **2018**, *9*, 155. [[CrossRef](#)]
72. Malaki, M.; Maleki, A.; Varma, R.S. MXenes and Ultrasonication. *J. Mater. Chem. A* **2019**, *7*, 10843–10857. [[CrossRef](#)]
73. Zhang, P.; Wang, F.; Yu, M.; Zhuang, X.; Feng, X. Two-Dimensional Materials for Miniaturized Energy Storage Devices: From Individual Devices to Smart Integrated Systems. *Chem. Soc. Rev.* **2018**, *47*, 7426–7451. [[PubMed](#)]
74. Hemanth, N.R.; Kandasubramanian, B. Recent Advances in 2D MXenes for Enhanced Cation Intercalation in Energy Harvesting Applications: A Review. *Chem. Eng. J.* **2020**, *392*, 123678.
75. Lukatskaya, M.R.; Kota, S.; Lin, Z.; Zhao, M.-Q.; Shpigel, N.; Levi, M.D.; Halim, J.; Taberna, P.-L.; Barsoum, M.W.; Simon, P. Ultra-High-Rate Pseudocapacitive Energy Storage in Two-Dimensional Transition Metal Carbides. *Nat. Energy* **2017**, *2*, 17105.

76. Li, X.; Bai, Y.; Shi, X.; Su, N.; Nie, G.; Zhang, R.; Nie, H.; Ye, L. Applications of MXene ( $\text{Ti}_3\text{C}_2\text{T}_x$ ) in Photocatalysis: A Review. *Mater. Adv.* **2021**, *2*, 1570–1594. [CrossRef]
77. Zhu, J.; Tang, Y.; Yang, C.; Wang, F.; Cao, M. Composites of  $\text{TiO}_2$  Nanoparticles Deposited on  $\text{Ti}_3\text{C}_2$  MXene Nanosheets with Enhanced Electrochemical Performance. *J. Electrochem. Soc.* **2016**, *163*, A785–A791. [CrossRef]
78. Ding, X.; Li, Y.; Li, C.; Wang, W.; Wang, L.; Feng, L.; Han, D. 2D Visible-Light-Driven  $\text{TiO}_2/\text{Ti}_3\text{C}_2/\text{g-C}_3\text{N}_4$  Ternary Heterostructure for High Photocatalytic Activity. *J. Mater. Sci.* **2019**, *54*, 9385–9396. [CrossRef]
79. Anasori, B.; Lukatskaya, M.R.; Gogotsi, Y. 2D Metal Carbides and Nitrides (MXenes) for Energy Storage. *Nat. Rev. Mater.* **2017**, *2*, 16098.
80. Chae, Y.; Kim, S.J.; Cho, S.-Y.; Choi, J.; Maleski, K.; Lee, B.-J.; Jung, H.-T.; Gogotsi, Y.; Lee, Y.; Ahn, C.W. An Investigation into the Factors Governing the Oxidation of Two-Dimensional  $\text{Ti}_3\text{C}_2$  MXene. *Nanoscale* **2019**, *11*, 8387–8393.
81. Li, K.; Wang, X.; Li, S.; Urbankowski, P.; Li, J.; Xu, Y.; Gogotsi, Y. An Ultrafast Conducting Polymer@MXene Positive Electrode with High Volumetric Capacitance for Advanced Asymmetric Supercapacitors. *Small* **2020**, *16*, e1906851. [CrossRef]
82. Hu, T.; Li, Z.; Hu, M.; Wang, J.; Hu, Q.; Li, Q.; Wang, X. Chemical Origin of Termination-Functionalized MXenes:  $\text{Ti}_3\text{C}_2\text{T}_2$  as a Case Study. *J. Phys. Chem. C* **2017**, *121*, 19254–19261.
83. Wang, D.D.; Tian, W.B.; Lu, C.J.; Ding, J.X.; Zhu, Y.F.; Zhang, M.; Zhang, P.G.; Sun, Z.M. Comparison of the Interfacial Reactions and Properties between  $\text{Ag}/\text{Ti}_3\text{AlC}_2$  and  $\text{Ag}/\text{Ti}_3\text{SiC}_2$  Electrical Contact Materials. *J. Alloys Compd.* **2021**, *857*, 157588. [CrossRef]
84. Son, W.; Gao, H.; Duong, T.; Talapatra, A.; Radovic, M.; Arróyave, R. Effect of A Mixing on Elastic Modulus, Cleavage Stress, and Shear Stress in the  $\text{Ti}_3(\text{Si}_x\text{Al}_{1-x})\text{C}_2$  MAX Phase. *Phys. Rev. B* **2017**, *95*, 235131. [CrossRef]
85. Husairi, F.S.; Eswar, K.A.; Azlinda, A.; Rusop, M.; Abdullah, S. Effect of Urea as a Stabiliser in the Thermal Immersion Method to Synthesise Zinc Oxide Nanostructures on Porous Silicon Nanostructures. *Adv. Mater. Res.* **2014**, *832*, 644–648. [CrossRef]
86. Wang, H.; Sun, Y.; Wu, Y.; Tu, W.; Wu, S.; Yuan, X.; Zeng, G.; Xu, Z.J.; Li, S.; Chew, J.W. Electrical Promotion of Spatially Photoinduced Charge Separation via Interfacial-Built-in Quasi-Alloying Effect in Hierarchical  $\text{Zn}_2\text{In}_2\text{S}_5/\text{Ti}_3\text{C}_2(\text{O}, \text{OH})_x$  Hybrids toward Efficient Photocatalytic Hydrogen Evolution and Environmental Remediation. *Appl. Catal. B Environ.* **2019**, *245*, 290–301.
87. Junkaew, A.; Arróyave, R. Enhancement of the Selectivity of MXenes ( $\text{M}_2\text{C}$ ,  $\text{M} = \text{Ti}, \text{V}, \text{Nb}, \text{Mo}$ ) via Oxygen-Functionalization: Promising Materials for Gas-Sensing and -Separation. *Phys. Chem. Chem. Phys.* **2018**, *20*, 6073–6082. [CrossRef] [PubMed]
88. Qian, Y.; Wei, H.; Dong, J.; Du, Y.; Fang, X.; Zheng, W.; Sun, Y.; Jiang, Z. Fabrication of Urchin-like  $\text{ZnO}$ -MXene Nanocomposites for High-Performance Electromagnetic Absorption. *Ceram. Int.* **2017**, *43*, 10757–10762. [CrossRef]
89. Zhao, Q.; Zhu, Q.; Miao, J.; Zhang, P.; Wan, P.; He, L.; Xu, B. Flexible 3D Porous MXene Foam for High-Performance Lithium-Ion Batteries. *Small* **2019**, *15*, e1904293. [CrossRef]
90. Zhang, M.; Qin, J.; Rajendran, S.; Zhang, X.; Liu, R. Heterostructured  $\text{D-Ti}_3\text{C}_2/\text{TiO}_2/\text{g-C}_3\text{N}_4$  Nanocomposites with Enhanced Visible-Light Photocatalytic Hydrogen Production Activity. *ChemSusChem* **2018**, *11*, 4226–4236. [CrossRef]
91. Gasso, S.; Mahajan, A. Development of Highly Sensitive and Humidity Independent Room Temperature  $\text{NO}_2$  Gas Sensor Using Two Dimensional  $\text{Ti}_3\text{C}_2\text{T}_x$  Nanosheets and One Dimensional  $\text{WO}_3$  Nanorods Nanocomposite. *ACS Sens.* **2022**, *7*, 2454–2464. [CrossRef]
92. Liu, X.; Zhang, H.; Song, Y.; Shen, T.; Sun, J. Facile Solvothermal Synthesis of  $\text{ZnO}/\text{Ti}_3\text{C}_2\text{T}_x$  MXene Nanocomposites for  $\text{NO}_2$  Detection at Low Working Temperature. *Sens. Actuators B Chem.* **2022**, *367*, 132025. [CrossRef]
93. Hantanasirisakul, K.; Gogotsi, Y. Electronic and Optical Properties of 2D Transition Metal Carbides and Nitrides (MXenes). *Adv. Mater.* **2018**, *30*, 1804779. [CrossRef] [PubMed]
94. Lipatov, A.; Alhabeb, M.; Lukatskaya, M.R.; Bosen, A.; Gogotsi, Y.; Sinitkii, A. Effect of Synthesis on Quality, Electronic Properties and Environmental Stability of Individual Monolayer  $\text{Ti}_3\text{C}_2$  MXene Flakes. *Adv. Electron. Mater.* **2016**, *2*, 1600255. [CrossRef]
95. Doan, T.H.P.; Hong, W.G.; Noh, J.-S. Palladium Nanoparticle-Decorated Multi-Layer  $\text{Ti}_3\text{C}_2\text{T}_x$  Dual-Functioning as a Highly Sensitive Hydrogen Gas Sensor and Hydrogen Storage. *RSC Adv.* **2021**, *11*, 7492–7501. [CrossRef]
96. Zhu, Z.; Liu, C.; Jiang, F.; Liu, J.; Ma, X.; Liu, P.; Xu, J.; Wang, L.; Huang, R. Flexible and Lightweight  $\text{Ti}_3\text{C}_2\text{T}_x$  MXene@ Pd Colloidal Nanoclusters Paper Film as Novel  $\text{H}_2$  Sensor. *J. Hazard. Mater.* **2020**, *399*, 123054. [CrossRef]
97. Nam, M.-S.; Kim, J.-Y.; Mirzaei, A.; Kim, H.W.; Kim, S.S. Self-Heated, Flexible, and Selective  $\text{H}_2$  Gas Sensors Based on Pd-Decorated  $\text{Ti}_3\text{C}_2\text{T}_x$  Mxenes. Available online: <http://dx.doi.org/10.2139/ssrn.4367681> (accessed on 26 June 2023).
98. Yuan, W.; Yang, K.; Peng, H.; Li, F.; Yin, F. A Flexible VOCs Sensor Based on a 3D Mxene Framework with a High Sensing Performance. *J. Mater. Chem. A* **2018**, *6*, 18116–18124. [CrossRef]
99. Sehab, N.; Amara, A.; Mebdoua, Y. Mechanical Activation-Assisted Electro-Thermal Explosion Synthesis of the  $\text{Ti}_2\text{AlC}$  Phase. *Mater. Manuf. Process.* **2017**, *32*, 1260–1264. [CrossRef]
100. Hermawan, A.; Zhang, B.; Taufik, A.; Asakura, Y.; Hasegawa, T.; Zhu, J.; Shi, P.; Yin, S.  $\text{CuO}$  Nanoparticles/ $\text{Ti}_3\text{C}_2\text{T}_x$  MXene Hybrid Nanocomposites for Detection of Toluene Gas. *ACS Appl. Nano Mater.* **2020**, *3*, 4755–4766. [CrossRef]
101. Liu, Z.; Lv, H.; Xie, Y.; Wang, J.; Fan, J.; Sun, B.; Jiang, L.; Zhang, Y.; Wang, R.; Shi, K. A 2D/2D/2D  $\text{Ti}_3\text{C}_2\text{T}_x/\text{TiO}_2/\text{MoS}_2$  Heterostructure as an Ultrafast and High-Sensitivity  $\text{NO}_2$  Gas Sensor at Room-Temperature. *J. Mater. Chem. A* **2022**, *10*, 11980–11989. [CrossRef]
102. He, T.; Liu, W.; Lv, T.; Ma, M.; Liu, Z.; Vasiliev, A.; Li, X. MXene/ $\text{SnO}_2$  Heterojunction Based Chemical Gas Sensors. *Sens. Actuators B Chem.* **2021**, *329*, 129275. [CrossRef]
103. Ta, Q.T.H.; Tri, N.N.; Noh, J.-S. Improved  $\text{NO}_2$  Gas Sensing Performance of 2D  $\text{MoS}_2/\text{Ti}_3\text{C}_2\text{T}_x$  MXene Nanocomposite. *Appl. Surf. Sci.* **2022**, *604*, 154624.

104. Zhang, D.; Mi, Q.; Wang, D.; Li, T. MXene/Co<sub>3</sub>O<sub>4</sub> Composite Based Formaldehyde Sensor Driven by ZnO/MXene Nanowire Arrays Piezoelectric Nanogenerator. *Sensors Actuators B Chem.* **2021**, *339*, 129923. [[CrossRef](#)]
105. Yang, Z.; Jiang, L.; Wang, J.; Liu, F.; He, J.; Liu, A.; Lv, S.; You, R.; Yan, X.; Sun, P. Flexible Resistive NO<sub>2</sub> Gas Sensor of Three-Dimensional Crumpled MXene Ti<sub>3</sub>C<sub>2</sub>T<sub>x</sub>/ZnO Spheres for Room Temperature Application. *Sens. Actuators B Chem.* **2021**, *326*, 128828. [[CrossRef](#)]
106. Guo, X.; Ding, Y.; Kuang, D.; Wu, Z.; Sun, X.; Du, B.; Liang, C.; Wu, Y.; Qu, W.; Xiong, L. Enhanced Ammonia Sensing Performance Based on MXene-Ti<sub>3</sub>C<sub>2</sub>T<sub>x</sub> Multilayer Nanoflakes Functionalized by Tungsten Trioxide Nanoparticles. *J. Colloid Interface Sci.* **2021**, *595*, 6–14. [[CrossRef](#)] [[PubMed](#)]
107. Zhao, L.; Wang, K.; Wei, W.; Wang, L.; Han, W. High-performance Flexible Sensing Devices Based on Polyaniline/MXene Nanocomposites. *InfoMat* **2019**, *1*, 407–416. [[CrossRef](#)]
108. Sun, S.; Wang, M.; Chang, X.; Jiang, Y.; Zhang, D.; Wang, D.; Zhang, Y.; Lei, Y. W<sub>18</sub>O<sub>49</sub>/Ti<sub>3</sub>C<sub>2</sub>T<sub>x</sub> MXene Nanocomposites for Highly Sensitive Acetone Gas Sensor with Low Detection Limit. *Sens. Actuators B Chem.* **2020**, *304*, 127274. [[CrossRef](#)]
109. Jin, L.; Wu, C.; Wei, K.; He, L.; Gao, H.; Zhang, H.; Zhang, K.; Asiri, A.M.; Alamry, K.A.; Yang, L. Polymeric Ti<sub>3</sub>C<sub>2</sub>T<sub>x</sub> MXene Composites for Room Temperature Ammonia Sensing. *ACS Appl. Nano Mater.* **2020**, *3*, 12071–12079. [[CrossRef](#)]
110. Liu, M.; Wang, Z.; Song, P.; Yang, Z.; Wang, Q. In<sub>2</sub>O<sub>3</sub> Nanocubes/Ti<sub>3</sub>C<sub>2</sub>T<sub>x</sub> MXene Composites for Enhanced Methanol Gas Sensing Properties at Room Temperature. *Ceram. Int.* **2021**, *47*, 23028–23037. [[CrossRef](#)]
111. Chen, T.; Yan, W.; Wang, Y.; Li, J.; Hu, H.; Ho, D. SnS<sub>2</sub>/MXene Derived TiO<sub>2</sub> Hybrid for Ultra-Fast Room Temperature NO<sub>2</sub> Gas Sensing. *J. Mater. Chem. C* **2021**, *9*, 7407–7416. [[CrossRef](#)]
112. Chen, W.Y.; Jiang, X.; Lai, S.-N.; Peroulis, D.; Stanciu, L. Nanohybrids of a MXene and Transition Metal Dichalcogenide for Selective Detection of Volatile Organic Compounds. *Nat. Commun.* **2020**, *11*, 1302. [[CrossRef](#)] [[PubMed](#)]
113. Lee, S.H.; Eom, W.; Shin, H.; Ambade, R.B.; Bang, J.H.; Kim, H.W.; Han, T.H. Room-Temperature, Highly Durable Ti<sub>3</sub>C<sub>2</sub>T<sub>x</sub> MXene/Graphene Hybrid Fibers for NH<sub>3</sub> Gas Sensing. *ACS Appl. Mater. Interfaces* **2020**, *12*, 10434–10442. [[CrossRef](#)] [[PubMed](#)]
114. Sun, B.; Lv, H.; Liu, Z.; Wang, J.; Bai, X.; Zhang, Y.; Chen, J.; Kan, K.; Shi, K. Co<sub>3</sub>O<sub>4</sub>@PEI/Ti<sub>3</sub>C<sub>2</sub>T<sub>x</sub> MXene Nanocomposites for a Highly Sensitive NO<sub>x</sub> Gas Sensor with a Low Detection Limit. *J. Mater. Chem. A* **2021**, *9*, 6335–6344. [[CrossRef](#)]
115. Zou, S.; Gao, J.; Liu, L.; Lin, Z.; Fu, P.; Wang, S.; Chen, Z. Enhanced Gas Sensing Properties at Low Working Temperature of Iron Molybdate/MXene Composite. *J. Alloys Compd.* **2020**, *817*, 152785. [[CrossRef](#)]
116. Gogotsi, Y.; Huang, Q. MXenes: Two-Dimensional Building Blocks for Future Materials and Devices. *ACS Nano* **2021**, *15*, 5775–5780. [[CrossRef](#)]
117. Lim, K.R.G.; Shekhirev, M.; Wyatt, B.C.; Anasori, B.; Gogotsi, Y.; Seh, Z.W. Fundamentals of MXene Synthesis. *Nat. Synth.* **2022**, *1*, 601–614. [[CrossRef](#)]
118. Lee, E.; VahidMohammadi, A.; Prorok, B.C.; Yoon, Y.S.; Beidaghi, M.; Kim, D.-J. Room Temperature Gas Sensing of Two-Dimensional Titanium Carbide (MXene). *ACS Appl. Mater. Interfaces* **2017**, *9*, 37184–37190. [[CrossRef](#)]
119. Majhi, S.M.; Ali, A.; Greish, Y.E.; El-Maghraby, H.F.; Qamhie, N.N.; Hajamohideen, A.R.; Mahmoud, S.T. Accordion-like-Ti<sub>3</sub>C<sub>2</sub> MXene-Based Gas Sensors with Sub-Ppm Level Detection of Acetone at Room Temperature. *ACS Appl. Electron. Mater.* **2022**, *4*, 4094–4103. [[CrossRef](#)]
120. Chen, W.Y.; Lai, S.-N.; Yen, C.-C.; Jiang, X.; Peroulis, D.; Stanciu, L.A. Surface Functionalization of Ti<sub>3</sub>C<sub>2</sub>T<sub>x</sub> MXene with Highly Reliable Superhydrophobic Protection for Volatile Organic Compounds Sensing. *ACS Nano* **2020**, *14*, 11490–11501. [[CrossRef](#)]
121. Shuvo, S.N.; Ulloa Gomez, A.M.; Mishra, A.; Chen, W.Y.; Dongare, A.M.; Stanciu, L.A. Sulfur-Doped Titanium Carbide MXenes for Room-Temperature Gas Sensing. *ACS Sens.* **2020**, *5*, 2915–2924. [[CrossRef](#)]
122. Li, D.; Qu, M.; Zhang, Q.; Xie, J. Multivariable Sensor Based on MXene and Machine Learning for Selective Detections of VOCs. In Proceedings of the 2021 IEEE 34th International Conference on Micro Electro Mechanical Systems (MEMS), Virtual, 25–29 January 2021; IEEE: Piscataway, NJ, USA, 2021; pp. 802–805.
123. Lee, E.; VahidMohammadi, A.; Yoon, Y.S.; Beidaghi, M.; Kim, D.-J. Two-Dimensional Vanadium Carbide MXene for Gas Sensors with Ultrahigh Sensitivity toward Nonpolar Gases. *ACS Sens.* **2019**, *4*, 1603–1611. [[CrossRef](#)] [[PubMed](#)]
124. Guo, W.; Surya, S.G.; Babar, V.; Ming, F.; Sharma, S.; Alshareef, H.N.; Schwingenschlogl, U.; Salama, K.N. Selective Toluene Detection with Mo<sub>2</sub>CT<sub>x</sub> MXene at Room Temperature. *ACS Appl. Mater. Interfaces* **2020**, *12*, 57218–57227. [[CrossRef](#)] [[PubMed](#)]
125. Vasseghian, Y.; Doan, V.D.; Nguyen, T.T.T.; Vo, T.-T.T.; Do, H.H.; Vu, K.B.; Vu, Q.H.; Dai Lam, T.; Tran, V.A. Flexible and High-Sensitivity Sensor Based on Ti<sub>3</sub>C<sub>2</sub>-MoS<sub>2</sub> MXene Composite for the Detection of Toxic Gases. *Chemosphere* **2022**, *291*, 133025.
126. Zhu, L.; Zeng, W. Room-Temperature Gas Sensing of ZnO-Based Gas Sensor: A Review. *Sens. Actuators A Phys.* **2017**, *267*, 242–261. [[CrossRef](#)]
127. Yang, D.; Fan, X.; Zhao, D.; An, Y.; Hu, Y.; Luo, Z. Sc<sub>2</sub>CO<sub>2</sub> and Mn-Doped Sc<sub>2</sub>CO<sub>2</sub> as Gas Sensor Materials to NO and CO: A First-Principles Study. *Phys. E Low-Dimens. Syst. Nanostruct.* **2019**, *111*, 84–90. [[CrossRef](#)]
128. Sun, L.; Sun, N.; Liu, Y.; Jiang, C. Anisotropic Frictional Properties between Ti<sub>3</sub>C<sub>2</sub>T<sub>x</sub> MXene/SiO<sub>2</sub> Layer-Dependent Heterojunctions. *J. Sci. Adv. Mater. Devices* **2021**, *6*, 488–493. [[CrossRef](#)]
129. Zhao, Q.-N.; Zhang, Y.-J.; Duan, Z.-H.; Wang, S.; Liu, C.; Jiang, Y.-D.; Tai, H.-L. A Review on Ti<sub>3</sub>C<sub>2</sub>T<sub>x</sub>-Based Nanomaterials: Synthesis and Applications in Gas and Humidity Sensors. *Rare Met.* **2021**, *40*, 1459–1476. [[CrossRef](#)]
130. Devaraj, M.; Rajendran, S.; Hoang, T.K.A.; Soto-Moscoso, M. A Review on MXene and Its Nanocomposites for the Detection of Toxic Inorganic Gases. *Chemosphere* **2022**, *302*, 134933. [[CrossRef](#)]

131. Ta, Q.T.H.; Thakur, D.; Noh, J.-S. Enhanced Gas Sensing Performance of ZnO/Ti<sub>3</sub>C<sub>2</sub>T<sub>x</sub> MXene Nanocomposite. *Micromachines* **2022**, *13*, 1710. [[CrossRef](#)]
132. Pazniak, H.; Plugin, I.A.; Loes, M.J.; Inerbaev, T.M.; Burmistrov, I.N.; Gorshenkov, M.; Polcak, J.; Varezchnikov, A.S.; Sommer, M.; Kuznetsov, D. V Partially Oxidized Ti<sub>3</sub>C<sub>2</sub>T<sub>x</sub> MXenes for Fast and Selective Detection of Organic Vapors at Part-per-Million Concentrations. *ACS Appl. Nano Mater.* **2020**, *3*, 3195–3204. [[CrossRef](#)]
133. Hou, M.; Guo, S.; Yang, L.; Gao, J.; Hu, T.; Wang, X.; Li, Y. Improvement of Gas Sensing Property for Two-Dimensional Ti<sub>3</sub>C<sub>2</sub>T<sub>x</sub> Treated with Oxygen Plasma by Microwave Energy Excitation. *Ceram. Int.* **2021**, *47*, 7728–7737. [[CrossRef](#)]
134. Wang, D.; Zhang, D.; Yang, Y.; Mi, Q.; Zhang, J.; Yu, L. Multifunctional Latex/Polytetrafluoroethylene-Based Triboelectric Nanogenerator for Self-Powered Organ-like MXene/Metal–Organic Framework-Derived CuO Nanohybrid Ammonia Sensor. *ACS Nano* **2021**, *15*, 2911–2919. [[CrossRef](#)] [[PubMed](#)]
135. Zheng, Q.; Shi, B.; Li, Z.; Wang, Z.L. Recent Progress on Piezoelectric and Triboelectric Energy Harvesters in Biomedical Systems. *Adv. Sci.* **2017**, *4*, 1700029. [[CrossRef](#)]
136. Ahmed, A.; Hassan, I.; El-Kady, M.F.; Radhi, A.; Jeong, C.K.; Selvaganapathy, P.R.; Zu, J.; Ren, S.; Wang, Q.; Kaner, R.B. Integrated Triboelectric Nanogenerators in the Era of the Internet of Things. *Adv. Sci.* **2019**, *6*, 1802230. [[CrossRef](#)]
137. Yang, Y.; Lin, L.; Zhang, Y.; Jing, Q.; Hou, T.-C.; Wang, Z.L. Self-Powered Magnetic Sensor Based on a Triboelectric Nanogenerator. *ACS Nano* **2012**, *6*, 10378–10383. [[CrossRef](#)]
138. Zhou, Y.; Deng, W.; Xu, J.; Chen, J. Engineering Materials at the Nanoscale for Triboelectric Nanogenerators. *Cell Reports Phys. Sci.* **2020**, *1*, 100142. [[CrossRef](#)]
139. Dong, Y.; Mallineni, S.S.K.; Maleski, K.; Behlow, H.; Mochalin, V.N.; Rao, A.M.; Gogotsi, Y.; Podila, R. Metallic MXenes: A New Family of Materials for Flexible Triboelectric Nanogenerators. *Nano Energy* **2018**, *44*, 103–110. [[CrossRef](#)]
140. Zhang, S.; Rana, S.M.S.; Bhatta, T.; Pradhan, G.B.; Sharma, S.; Song, H.; Jeong, S.; Park, J.Y. 3D Printed Smart Glove with Pyramidal MXene/Ecoflex Composite-Based Toroidal Triboelectric Nanogenerators for Wearable Human-Machine Interaction Applications. *Nano Energy* **2023**, *106*, 108110. [[CrossRef](#)]
141. Chang, L.; Xiao, X. The Review of MXenes for Osmotic Energy Harvesting: Synthesis and Properties. *Diam. Relat. Mater.* **2023**, *136*, 109971. [[CrossRef](#)]
142. Luo, X.; Zhu, L.; Wang, Y.; Li, J.; Nie, J.; Wang, Z.L. A Flexible Multifunctional Triboelectric Nanogenerator Based on MXene/PVA Hydrogel. *Adv. Funct. Mater.* **2021**, *31*, 2104928. [[CrossRef](#)]
143. Cao, W.; Ouyang, H.; Xin, W.; Chao, S.; Ma, C.; Li, Z.; Chen, F.; Ma, M. A Stretchable Highoutput Triboelectric Nanogenerator Improved by MXene Liquid Electrode with High Electronegativity. *Adv. Funct. Mater.* **2020**, *30*, 2004181. [[CrossRef](#)]
144. Kim, K.N.; Kim, S.Y.; Choi, S.H.; Lee, M.; Song, W.; Lim, J.; Lee, S.S.; Myung, S. All-Printed Wearable Triboelectric Nanogenerator with Ultra-Charged Electron Accumulation Polymers Based on MXene Nanoflakes. *Adv. Electron. Mater.* **2022**, *8*, 2200819. [[CrossRef](#)]
145. Rana, S.M.S.; Rahman, M.T.; Salauddin, M.; Sharma, S.; Maharjan, P.; Bhatta, T.; Cho, H.; Park, C.; Park, J.Y. Electrospun PVDF-TrFE/MXene Nanofiber Mat-Based Triboelectric Nanogenerator for Smart Home Appliances. *ACS Appl. Mater. Interfaces* **2021**, *13*, 4955–4967. [[CrossRef](#)] [[PubMed](#)]
146. Tan, D.; Sun, N.; Chen, L.; Bu, J.; Jiang, C. Piezoelectricity in Monolayer and Multilayer Ti<sub>3</sub>C<sub>2</sub>T<sub>x</sub> MXenes: Implications for Piezoelectric Devices. *ACS Appl. Nano Mater.* **2021**, *5*, 1034–1046. [[CrossRef](#)]
147. Cao, V.A.; Kim, M.; Lee, S.; Kim, C.G.; Cao Van, P.; Thi, T.N.; Jeong, J.-R.; Nah, J. Enhanced Output Performance of a Flexible Piezoelectric Nanogenerator Realized by Lithium-Doped Zinc Oxide Nanowires Decorated on MXene. *ACS Appl. Mater. Interfaces* **2022**, *14*, 26824–26832. [[CrossRef](#)] [[PubMed](#)]
148. Han, C.; Zhang, H.; Chen, Q.; Li, T.; Kong, L.; Zhao, H.; He, L. A Directional Piezoelectric Sensor Based on Anisotropic PVDF/MXene Hybrid Foam Enabled by Unidirectional Freezing. *Chem. Eng. J.* **2022**, *450*, 138280. [[CrossRef](#)]
149. Auliya, R.Z.; Ooi, P.C.; Sadri, R.; Talik, N.A.; Yau, Z.Y.; Mohammad Haniff, M.A.S.; Goh, B.T.; Dee, C.F.; Aslfattahi, N.; Al-Bati, S. Exploration of 2D Ti<sub>3</sub>C<sub>2</sub> MXene for All Solution Processed Piezoelectric Nanogenerator Applications. *Sci. Rep.* **2021**, *11*, 17432. [[CrossRef](#)]
150. Chang, W.-L.; Sun, Z.-Q.; Zhang, Z.-M.; Wei, X.-P.; Tao, X. Thermoelectric Properties of Two-Dimensional Double Transition Metal MXenes: ScYCT<sub>2</sub> (T = F, OH). *J. Phys. Chem. Solids* **2023**, *176*, 111210. [[CrossRef](#)]
151. Bark, H.; Thangavel, G.; Liu, R.J.; Chua, D.H.C.; Lee, P.S. Effective Surface Modification of 2D MXene toward Thermal Energy Conversion and Management. *Small Methods* **2023**, *7*, 2300077. [[CrossRef](#)]
152. Fei, J.; Koh, S.W.; Tu, W.; Ge, J.; Rezaeyan, H.; Hou, S.; Duan, H.; Lam, Y.C.; Li, H. Functionalized MXene Enabled Sustainable Water Harvesting and Desalination. *Adv. Sustain. Syst.* **2020**, *4*, 2000102. [[CrossRef](#)]
153. Zhao, K.; Lee, J.W.; Yu, Z.G.; Jiang, W.; Oh, J.W.; Kim, G.; Han, H.; Kim, Y.; Lee, K.; Lee, S. Humidity-Tolerant Moisture-Driven Energy Generator with MXene Aerogel–Organohydrogel Bilayer. *ACS Nano* **2023**, *17*, 5472–5485. [[CrossRef](#)] [[PubMed](#)]
154. Bae, J.; Kim, M.S.; Oh, T.; Suh, B.L.; Yun, T.G.; Lee, S.; Hur, K.; Gogotsi, Y.; Koo, C.M.; Kim, I.-D. Towards Watt-Scale Hydroelectric Energy Harvesting by Ti<sub>3</sub>C<sub>2</sub>T<sub>x</sub>-Based Transpiration-Driven Electrokinetic Power Generators. *Energy Environ. Sci.* **2022**, *15*, 123–135. [[CrossRef](#)]
155. Li, P.; Su, N.; Wang, Z.; Qiu, J. A Ti<sub>3</sub>C<sub>2</sub>T<sub>x</sub> MXene-Based Energy-Harvesting Soft Actuator with Self-Powered Humidity Sensing and Real-Time Motion Tracking Capability. *ACS Nano* **2021**, *15*, 16811–16818. [[CrossRef](#)] [[PubMed](#)]

156. Kim, J.Y.; Lee, J.-W.; Jung, H.S.; Shin, H.; Park, N.-G. High-Efficiency Perovskite Solar Cells. *Chem. Rev.* **2020**, *120*, 7867–7918. [[CrossRef](#)] [[PubMed](#)]
157. Guo, Z.; Gao, L.; Xu, Z.; Teo, S.; Zhang, C.; Kamata, Y.; Hayase, S.; Ma, T. High Electrical Conductivity 2D MXene Serves as Additive of Perovskite for Efficient Solar Cells. *Small* **2018**, *14*, 1802738. [[CrossRef](#)]
158. Zheng, H.; Wang, Y.; Niu, B.; Ge, R.; Lei, Y.; Yan, L.; Si, J.; Zhong, P.; Ma, X. Controlling the Defect Density of Perovskite Films by MXene/SnO<sub>2</sub> Hybrid Electron Transport Layers for Efficient and Stable Photovoltaics. *J. Phys. Chem. C* **2021**, *125*, 15210–15222. [[CrossRef](#)]
159. Wang, Y.; Xiang, P.; Ren, A.; Lai, H.; Zhang, Z.; Xuan, Z.; Wan, Z.; Zhang, J.; Hao, X.; Wu, L. MXene-Modulated Electrode/SnO<sub>2</sub> Interface Boosting Charge Transport in Perovskite Solar Cells. *ACS Appl. Mater. Interfaces* **2020**, *12*, 53973–53983. [[CrossRef](#)]
160. Shin, E.-Y.; Choi, S.B.; Lee, J.H.; Yoo, B.; Han, C.J.; Park, S.H.; Noh, J.H.; Kim, J.-W.; Son, H.J. An Inverted Layer-by-Layer Process to Enable Ultrasoft MXene–Ag Nanowire Hybrid Electrode for Organic Photovoltaics. *Sol. RRL* **2023**, *7*, 2201130. [[CrossRef](#)]
161. Chen, Y.; Wang, D.; Lin, Y.; Zou, X.; Xie, T. In Suit Growth of CuSe Nanoparticles on MXene (Ti<sub>3</sub>C<sub>2</sub>) Nanosheets as an Efficient Counter Electrode for Quantum Dot-Sensitized Solar Cells. *Electrochim. Acta* **2019**, *316*, 248–256. [[CrossRef](#)]
162. Aryal, U.K.; Pazniak, H.; Kumari, T.; Weber, M.; Johansson, F.O.L.; Vannucchi, N.; Witkowski, N.; Turkovic, V.; Di Carlo, A.; Madsen, M. 2D MXene-Based Electron Transport Layers for Nonhalogenated Solvent-Processed Stable Organic Solar Cells. *ACS Appl. Energy Mater.* **2023**, *6*, 4549–4558. [[CrossRef](#)]

**Disclaimer/Publisher’s Note:** The statements, opinions and data contained in all publications are solely those of the individual author(s) and contributor(s) and not of MDPI and/or the editor(s). MDPI and/or the editor(s) disclaim responsibility for any injury to people or property resulting from any ideas, methods, instructions or products referred to in the content.